



---

Year: 2010

---

## **The metal-binding properties of the blue crab copper specific CuMT-2: a crustacean metallothionein with two cysteine triplets**

Serra-Batiste, M ; Cols, N ; Alcaraz, L A ; Donaire, A ; González-Duarte, P ; Vasák, M

**Abstract:** Most crustacean metallothioneins (MTs) contain 18 Cys residues and bind six divalent metal ions. The copper-specific CuMT-2 (MTC) of the blue crab *Callinectes sapidus* with 21 Cys residues, of which six are organized in two uncommon Cys-Cys-Cys sequences, represents an exception. However, its metal-binding properties are unknown. By spectroscopic and spectrometric techniques we show that all 21 Cys residues of recombinant MTC participate in the binding of Cu(I), Zn(II), and Cd(II) ions, indicating that both Cys triplets act as ligands. The fully metallated M(8) (II)-MTC (M is Zn, Cd) form possesses high- and low-affinity metal binding sites, as evidenced by the formation of Zn(6)-MTC and Cd(7)-MTC species from M(8) (II)-MTC after treatment with Chelex 100. The NMR characterization of Cd(7)-MTC suggests the presence of a two-domain structure, each domain containing one Cys triplet and encompassing either the three-metal or the four-metal thiolate cluster. Whereas the metal-Cys connectivities in the three-metal cluster located in the N-terminal domain (residues 1-31) reveal a Cd(3)Cys(9) cyclohexane-like structure, the presence of dynamic processes in the C-terminal domain (residues 32-64) precluded the determination of the organization of the four-metal cluster. Absorption and circular dichroism features accompanying the stepwise binding of Cu(I) to MTC suggest that all 21 Cys are involved in the binding of eight to nine Cu(I) ions (Cu(8-9)-MTC). The subsequent generation of Cu(12)-MTC involves structural changes consistent with a decrease in the Cu(I) coordination number. Overall, the metal-binding properties of MTC reported here contribute to a better understanding of the role of Cys triplets in MTs.

DOI: <https://doi.org/10.1007/s00775-010-0644-z>

Posted at the Zurich Open Repository and Archive, University of Zurich

ZORA URL: <https://doi.org/10.5167/uzh-34629>

Journal Article

Published Version

Originally published at:

Serra-Batiste, M; Cols, N; Alcaraz, L A; Donaire, A; González-Duarte, P; Vasák, M (2010). The metal-binding properties of the blue crab copper specific CuMT-2: a crustacean metallothionein with two cysteine triplets. *Journal of Biological Inorganic Chemistry*, 15(5):759-776.

DOI: <https://doi.org/10.1007/s00775-010-0644-z>

# The metal-binding properties of the blue crab copper specific CuMT-2: a crustacean metallothionein with two cysteine triplets

Montserrat Serra-Batiste · Neus Cols ·  
Luis A. Alcaraz · Antonio Donaire ·  
Pilar González-Duarte · Milan Vašák

Received: 4 November 2009 / Accepted: 24 February 2010 / Published online: 2 April 2010  
© SBIC 2010

**Abstract** Most crustacean metallothioneins (MTs) contain 18 Cys residues and bind six divalent metal ions. The copper-specific CuMT-2 (MTC) of the blue crab *Callinectes sapidus* with 21 Cys residues, of which six are organized in two uncommon Cys-Cys-Cys sequences, represents an exception. However, its metal-binding properties are unknown. By spectroscopic and spectrometric techniques we show that all 21 Cys residues of recombinant MTC participate in the

binding of Cu(I), Zn(II), and Cd(II) ions, indicating that both Cys triplets act as ligands. The fully metallated  $M_8^{II}$ -MTC (M is Zn, Cd) form possesses high- and low-affinity metal binding sites, as evidenced by the formation of  $Zn_6$ -MTC and  $Cd_7$ -MTC species from  $M_8^{II}$ -MTC after treatment with Chelex 100. The NMR characterization of  $Cd_7$ -MTC suggests the presence of a two-domain structure, each domain containing one Cys triplet and encompassing either the three-metal or the four-metal thiolate cluster. Whereas the metal-Cys connectivities in the three-metal cluster located in the N-terminal domain (residues 1–31) reveal a  $Cd_3Cys_9$  cyclohexane-like structure, the presence of dynamic processes in the C-terminal domain (residues 32–64) precluded the determination of the organization of the four-metal cluster. Absorption and circular dichroism features accompanying the stepwise binding of Cu(I) to MTC suggest that all 21 Cys are involved in the binding of eight to nine Cu(I) ions ( $Cu_{8-9}$ -MTC). The subsequent generation of  $Cu_{12}$ -MTC involves structural changes consistent with a decrease in the Cu(I) coordination number. Overall, the metal-binding properties of MTC reported here contribute to a better understanding of the role of Cys triplets in MTs.

**Electronic supplementary material** The online version of this article (doi:10.1007/s00775-010-0644-z) contains supplementary material, which is available to authorized users.

M. Serra-Batiste · P. González-Duarte (✉)  
Departament de Química, Facultat de Ciències,  
Universitat Autònoma de Barcelona,  
08193 Bellaterra, Barcelona, Spain  
e-mail: pilar.gonzalez.duarte@uab.cat

N. Cols  
Departament de Genètica,  
Facultat de Biologia, Universitat de Barcelona,  
Av. Diagonal, 645, 08028 Barcelona, Spain

L. A. Alcaraz  
Departamento de Química Física,  
Facultad de Ciencias, Universidad de Alicante,  
03080 Alicante, Spain

A. Donaire  
Departamento de Química Inorgánica,  
Facultad de Química,  
Universidad de Murcia,  
30100 Murcia, Spain

M. Vašák (✉)  
Department of Biochemistry,  
University of Zurich,  
8057 Zurich, Switzerland  
e-mail: mvasak@bioc.uzh.ch

**Keywords** Metallothionein · Metal-thiolate clusters · Zinc · Cadmium · Copper

## Introduction

Metallothioneins (MTs) comprise a wide family of ubiquitous proteins with features that are exceptional from the perspectives of both the biology and the coordination chemistry. When compared with all other metalloproteins, MTs are wholly unconventional because of their small size (most of them are between 4 and 7 kDa), their high Cys

and metal content, and the lack of tertiary structure in their apo form (apoMT or thionein). Within the context of coordination chemistry, MTs are also unique in that they can form metal centers with different numbers of metals and nature, features reflecting the influence of the polypeptide chain on the ligation modes of thiolate sulfur. Another striking property of these proteins is the coexistence of different coordination geometries, even for the same metal ion. Apart from these remarkable structural properties, the biological function of MTs is the subject of intense research. Currently, they are considered as multifunctional proteins, playing major roles in metal detoxification and homeostatic trace element regulation, protection of cells against oxidative stress, radical scavenging, and organism growth and development [1, 2].

Two different cluster arrangements for divalent metal ions have been structurally characterized: an  $M_3Cys_9$  cluster contained in the  $\beta$ -domain of vertebrate, crustacean, and echinoderm MTs, and an  $M_4Cys_{11}$  cluster contained in the  $\alpha$ -domain of vertebrate and echinoderm MTs [1, 2]. A variant of the four metal ion cluster in which two His residues participate in metal coordination giving rise to an  $M_4Cys_9His_2$  cluster has been reported for MT from cyanobacteria [3]. Recently, the NMR solution structure of a plant MT has provided evidence for an unprecedented mononuclear binding site consisting of Zn(II) tetrahedrally coordinated by two Cys and two His residues, as found in certain zinc-finger motifs [4].

Until quite recently, the most remarkable feature of the primary structure of all MTs was the occurrence of Cys-Cys, Cys-X-Cys, and Cys-X-X-Cys structural motifs, where X stands for an amino acid residue other than Cys. Remarkably, in the last few years, MTs containing from one to six Cys-Cys-Cys tripeptide sequences have been isolated from several organisms. Their genes are induced

by different metal ions and both their total length and their Cys content vary significantly [5–12]. In the absence of 3D structural data for these novel MTs, the participation of the extra Cys present in the Cys triplets in metal binding has been ruled out for human, worm, and lobster isoforms [5–7], but has been proposed for a protozoan MT [13].

Compared with vertebrates, crustacean MTs have a peptide chain length of 58 to 59 amino acids, with a metal and Cys content of  $M_6^{II}$ -MT and 18 Cys per MT, respectively, instead of  $M_7^{II}$ -MT and 20 Cys per MT [14, 15]. The alignment of crustacean MT sequences illustrates their high sequence similarity, the only exceptions being those of *Portunus pelagicus* and the copper-specific *Callinectes sapidus* (Fig. 1). Remarkably, these two MTs contain two Cys triplets and show almost identical primary structures, which differ significantly from those of other crustacean MTs.

Within the context of our previous work on crustacean MTs, we now report on the recombinant synthesis and coordinating ability of the copper-specific *C. sapidus* MT (CuMT-2), denoted here as MTC. This protein is one of the three isoforms identified in the blue crab *C. sapidus* and, unlike the other two isoforms MT-1 and MT-2, is only induced by copper ions. The metal-binding properties and structural features reported for MT-1 and MT-2 compare well with those of other crustacean MTs. However, since marine crustaceans have a very dynamic copper metabolism associated with the synthesis and degradation of their respiratory protein hemocyanin, whose concentration is dependent on the molt cycle [16], it has been hypothesized that MTC could be involved in copper homeostasis associated with both the synthesis and the degradation of hemocyanin. Recently, in the analysis of the gene expression pattern of the crayfish *Cherax quadricarinatus* during the molt cycle, the presence of a new MT sequence

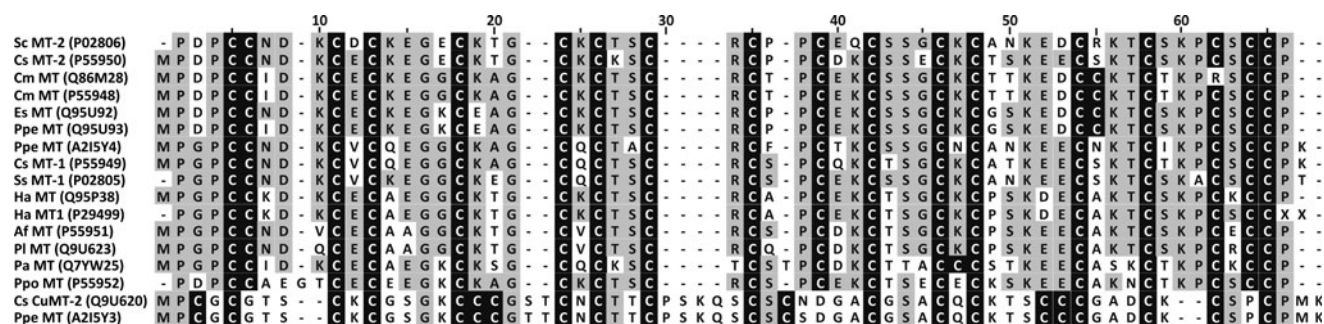


**Fig. 1** Multiple alignment analysis of a representative selection of crustacean metallothioneins (MTs). ClustalW-aligned MT sequences of the following organisms: *Scylla serrata* (Sc), *Callinectes sapidus* (Cs), *Carcinus maenas* (Cm), *Eriocheir sinensis* (Es), *Portunus pelagicus* (Ppe), *Homarus americanus* (Ha), *Astacus fluviatilis* (Af), *Pacifastacus leniusculus* (Pl), *Panulirus argus* (Pa), *Potamon*

*potamios* (Ppo). The corresponding accession numbers in Swiss-Prot are given in parentheses. Throughout this paper, Cs MT-1, Cs MT-2, and Cs CuMT-2 are denoted as MT-1, MT-2, and MTC, respectively. Cys residues are depicted in black and highly conserved positions in gray

containing Cys triplets and showing a high sequence similarity with the copper-specific *C. sapidus* MTC has also been described [17]. Therefore, the chemical characterization of the unconventional crustacean MTC protein should shed light on the role of Cys triplets in this class of metal-binding proteins.

## Results and discussion

### Expression and purification of recombinant Zn–MTC

The MTC complementary DNA (cDNA) was cloned into pGEX-4T-1 expression vector, as described in “[Materials and methods](#).” The integrity and accuracy of the amplified cDNA was confirmed by DNA sequencing. Although the method of expression of MTs in *Escherichia coli* is well established in our group [18], and has been successfully applied in recombinant synthesis of MTs from different organisms, it usually affords low yields [7, 19]. To increase the average yield of 0.5 mg l<sup>−1</sup> of bacterial culture, the expression conditions were varied. Among those, the addition of the corresponding metal to culture medium after 90 min of induction, instead of the standard 30 min, allowed us to recover about 1.5 mg l<sup>−1</sup> of the protein.

MTC was expressed and purified as the zinc protein. This is usually a fairly stable metalloform and, unlike redox-active copper, is not affected by the presence of oxygen. The presence of a single mass peak of 6,422 Da in the electrospray ionization mass spectrometry (ESI-MS) spectrum of the apoMTC (calculated mass 6,421.5 Da), obtained after acidification of the Zn–MTC form, established the correctness of the recombinant protein. This mass includes the two additional N-terminal amino acid residues Gly and Ser artificially introduced by the cloning strategy. Previously, we showed that their presence does not interfere with the metal-binding capabilities of MTs [20].

The characterization of the recombinant Zn–MTC by inductively coupled plasma atomic emission spectroscopy (ICP-AES) showed a Zn-to-MTC ratio of 5.2, which differs from the stoichiometry of the Zn–MTC species obtained by ESI-MS. In these studies, the presence of a mixture of Zn<sub>x</sub>–MTC complexes, where  $x = 6–8$ , was obtained with Zn<sub>6</sub>–MTC and Zn<sub>7</sub>–MTC being the main species (Table 1). As the presence of sulfide ions was discarded on the basis of ICP-AES analysis of acid pretreated samples [21], oxidation of some Cys residues may account for the discrepancy between the ICP-AES and ESI-MS results. However, attempts to determine the degree of oxidation by Ellman’s method [22] were unsuccessful owing most likely to differences in the composition of a mixture of Zn<sub>x</sub>–MTC complexes.

**Table 1** Characterization of the recombinant holo form of copper-specific *Callinectes sapidus* metallothionein (MTC) obtained in media supplemented with zinc, copper, or a mixture of both zinc and copper

Zinc-supplemented medium (300 μM ZnCl <sub>2</sub> )			
ICP-AES		ESI-MS	
5.2 Zn/MTC		Zn <sub>6–8</sub> –MTC <sup>a</sup>	
Copper-supplemented medium (500 μM CuSO <sub>4</sub> )			
Homometallic species		Heterometallic species	
ICP-AES	ESI-MS	ICP-AES	ESI-MS
11 Cu/MTC	Cu <sub>12–14</sub> –MTC <sup>a</sup>	6 Cu/MTC 2–3 Zn/MTC	M <sub>8–13</sub> –MTC <sup>b</sup>
Zinc- and copper-supplemented medium (300 μM ZnCl <sub>2</sub> and 500 μM CuSO <sub>4</sub> )			
Homometallic species		Heterometallic species	
ICP-AES	ESI-MS	ICP-AES	ESI-MS
11 Cu/MTC	Cu <sub>11–14</sub> –MTC <sup>a</sup>	5 Cu/MTC 3 Zn/MTC	M <sub>8–13</sub> –MTC <sup>b</sup>

ICP-AES inductively coupled plasma atomic emission spectroscopy, ESI-MS electrospray ionization mass spectrometry

<sup>a</sup> Mixture of species with stoichiometries within the range indicated

<sup>b</sup> Within the range indicated, M<sub>8</sub> and M<sub>12</sub> are predominant; on the basis of ESI-MS data it cannot be concluded whether M is Zn or Cu

### Characterization of reconstituted Zn–MTC

To gain insight into the stoichiometry of Zn(II) binding to MTC, the apoprotein was reconstituted with Zn(II) ions. The reconstitution procedure usually affords a well-defined MT species. However, analogously to the recombinant expression, the reconstitution of apoMTC with 8.5 mol equiv of ZnCl<sub>2</sub> led to a mixture of complexes Zn<sub>x</sub>–MTC,  $x = 6–8$ , whose main characteristics compare well with those obtained from the recombinant synthesis (Tables 1, 2). The thiolate quantification through the reaction with 2,2′-dithiopyridine (DTP) revealed that all protein thiolates are present in their reduced state (an oxidation degree of less than 5%). The presence of a mixture of metalloforms indicates that MTC possesses rather unusual metal-coordinating features. Remarkably, treatment of the reconstituted sample with the chelating resin Chelex 100 resulted essentially in a single Zn<sub>6</sub>–MTC species (Table 2). The reversibility of this process was ascertained by adding 2 mol equiv of Zn(II) to Zn<sub>6</sub>–MTC, which, according to ESI-MS, reestablished the initial Zn<sub>x</sub>–MTC,  $x = 6–8$ , mixture of species (Fig. 2). This indicates that in MTC six primary high-affinity Zn(II) binding sites and two low-affinity sites exist. The reversible binding of one additional divalent metal ion has also been reported in other crustacean MTs not containing Cys triplets. In this case, the participation of non-sulfur ligands in metal binding has been inferred [19, 23].

**Table 2** Analysis of apoMTC after reconstitution with Zn(II) and Cd(II)

Reconstituted Zn–MTC	
ICP-AES	ESI-MS
$6.4 \pm 0.2$ Zn/MTC	$\text{Zn}_{6-8}\text{-MTC}^{\text{a}}$ ( $\text{Zn}_6\text{-MTC}$ ) <sup>b</sup>
Reconstituted Cd–MTC	
ICP-AES	ESI-MS
$7.8 \pm 0.8$ Cd/MTC	$\text{Cd}_8\text{-MTC}$ ( $\text{Cd}_7\text{-MTC}$ ) <sup>c</sup>

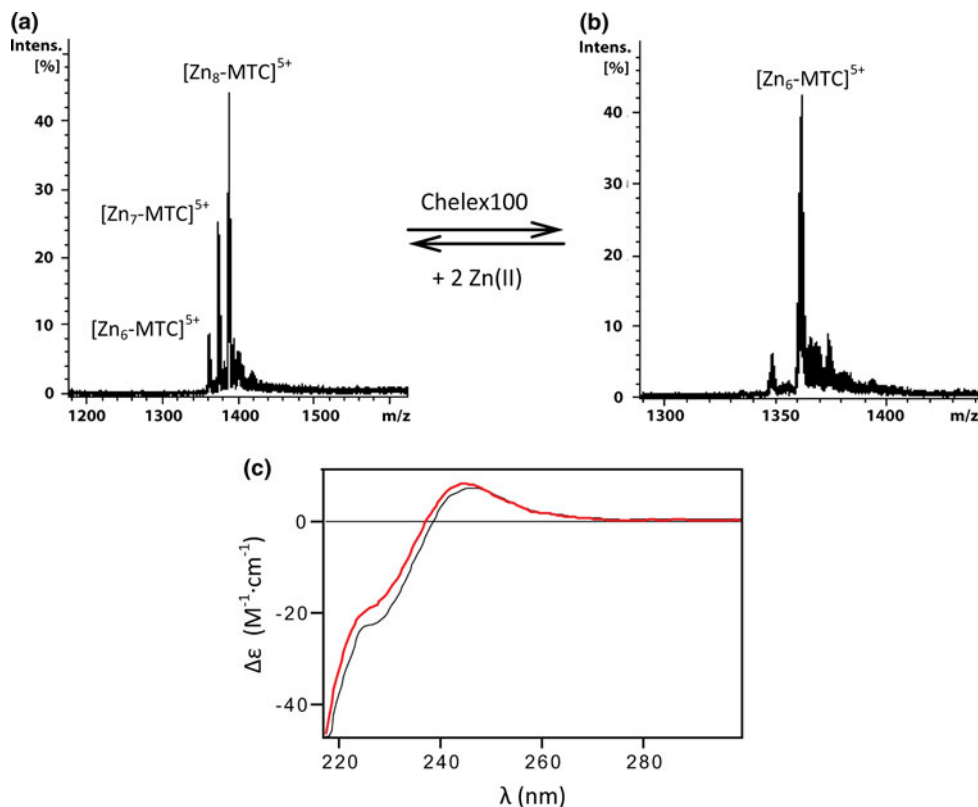
<sup>a</sup> Mixture of species with stoichiometries within the range indicated<sup>b</sup> Species observed after Chelex 100 treatment of the reconstituted  $\text{Zn}_{6-8}\text{-MTC}$  sample<sup>c</sup> Species observed after Chelex 100 treatment of the reconstituted  $\text{Cd}_8\text{-MTC}$  sample

Next we addressed the question of whether the  $\text{Zn}_6\text{-MTC}$  form contains uncoordinated Cys residues. We took advantage of the absorption band of deprotonated sulphhydryl groups at 237 nm. The difference absorption spectra of a solution of  $\text{Zn}_6\text{-MTC}$  at pH 7.4 titrated with increasing NaOH concentrations showed a band at 237 nm with a maximum absorption at pH 11.2 (Fig. S1). The molar absorptivity of this band divided by the determined molar extinction coefficient per Cys ( $\epsilon_{237} = 5 \times 10^3 \text{ M}^{-1} \text{ cm}^{-1}$ ) revealed the presence of two unbound Cys in  $\text{Zn}_6\text{-MTC}$ .

Up to now, the only canonical stoichiometry reported for crustacean MTs in complex with divalent metal ions is  $\text{M}_6^{\text{II}}\text{-MT}$ , where the standard content of Cys residues is 18 [15]. However, the crustacean MTC protein contains 21 Cys residues, six of them arranged in two rather uncommon Cys triplets. Owing to the increased number of Cys residues, the protein has the capability of forming the  $\text{Zn}_x\text{-MTC}$  complexes, where  $x = 6\text{--}8$ . Interestingly, the presence of two free Cys residues in  $\text{Zn}_6\text{-MTC}$  corresponds to the number of Cys triplets present in the primary structure, implying that one Cys of each triplet may serve as a ligand for the binding of the last two Zn(II) ions.

The circular dichroism (CD) spectra of  $\text{Zn}_6\text{-MTC}$  and  $\text{Zn}_{6-8}\text{-MTC}$  are shown in Fig. 2. As the aromatic amino acids are absent from MTC, the CD features originate mainly from the CysS–Zn(II) ligand to metal charge transfer (LMCT) transitions. By analogy to previous CD studies of Zn–MTs from various species, a biphasic CD profile of  $\text{Zn}_{6-8}\text{-MTC}$  with bands at (–)225 and (+)245 nm and a crossover point at 239 nm originate from the excitonically coupled transition dipole moments of the bridging thiolate ligands in a cluster structure. Thus, in  $\text{Zn}_{6-8}\text{-MTC}$  a cluster structure exists. Comparison of the CD features of  $\text{Zn}_6\text{-MTC}$  and  $\text{Zn}_{6-8}\text{-MTC}$  reveals that the binding of two additional Zn(II) ions is accompanied by only a minor perturbation of the original cluster structure in  $\text{Zn}_6\text{-MTC}$ . A small increase

**Fig. 2** Electrospray ionization mass spectrometry (ESI-MS) (a, b) and circular dichroism (CD) (c) spectra of Zn–MTC samples. **a** ApoMTC after reconstitution with Zn(II) yields a mixture of  $\text{Zn}_{6-8}\text{-MTC}$  species; **b** subsequent treatment of this sample with Chelex100 affords  $\text{Zn}_6\text{-MTC}$ , which evolves into the initial  $\text{Zn}_{6-8}\text{-MTC}$  mixture after addition of 2 mol equiv of Zn(II); **c** CD spectrum of the  $\text{Zn}_{6-8}\text{-MTC}$  sample (black line) compared with that of the  $\text{Zn}_6\text{-MTC}$  species obtained after Chelex 100 treatment (red line). The complete ESI-MS spectrum of  $\text{Zn}_6\text{-MTC}$  is shown in Fig. S6. Theoretical and experimental masses are detailed in Table S1





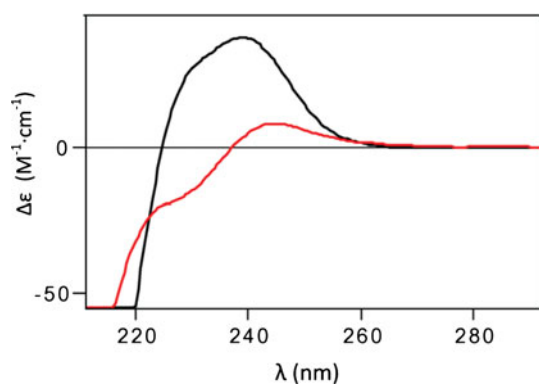


**Fig. 3** Comparison of the CD spectra of the  $\text{Zn}_6$ -MTC species obtained from reconstituted  $\text{Zn}_{6-8}$ -MTC after Chelex 100 treatment (red line) with crustacean *H. americanus*  $\text{Zn}_6$ -MTC (black line) [19]

in intensity of the CD band at 225 nm, observed upon the binding of eight Zn(II) to MTC, is due most likely to small changes in the peptide backbone contributions. Comparison of the CD features of the cluster structure present in  $\text{Zn}_6$ -MTC with those reported for  $\text{Zn}_6$ -MT from the crab *Homarus americanus* [15], containing two of the  $\text{M}_3^{\text{II}}\text{Cys}_9$  clusters, shows marked differences consistent with a substantially different cluster structure in  $\text{Zn}_6$ -MTC (Fig. 3).

#### Characterization of recombinant MTC synthesized in copper- and copper/zinc-enriched media

MTC is specifically induced by copper in the blue crab [11], where it plays a role in copper homeostasis [24]. These data suggest a particular adaptation of this MT to bind copper(I) compared with divalent metal ions. To gain insight into the binding properties of MTC toward Cu(I) ions, the protein was expressed in copper-enriched medium. Surprisingly, although all expression experiments were performed in culture medium enriched only with copper, either homometallic Cu-MTC or heterometallic Cu,Zn-MTC complexes were recovered in independent preparations (Table 1). The presence of zinc, which accounts for the formation of the heterometallic species, cannot be avoided because of the composition of standard culture medium. To evaluate the role of zinc in the heterometallic Cu,Zn-MTC, MTC was expressed in medium enriched with both copper and zinc. However, also in this case either homometallic Cu-MTC or heterometallic Cu,Zn-MTC complexes were isolated with metal-to-MTC stoichiometries comparable to those obtained in copper-enriched medium (Table 1). Overall, regardless of the origin of the  $\text{Cu}_x$ -MTC and  $\text{Cu}_x\text{Zn}_y$ -MTC forms, the ESI-MS data allow the following generalizations: (1) the stoichiometry of the various coexisting copper homometallic species in  $\text{Cu}_x$ -MTC corresponds mainly to  $x = 12$ –14 and (2) for the heterometallic  $\text{Cu}_x\text{Zn}_y$ -MTC species (further

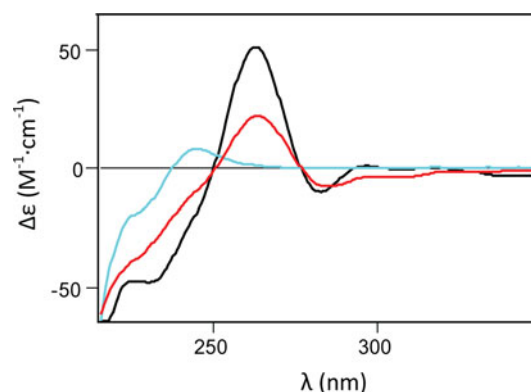


**Fig. 4** CD spectra of  $\text{Zn}_6$ -MTC (blue line),  $\text{Cu}_8$ -MTC (red line), and  $\text{Cu}_8\text{Zn}_4$ -MTC (black line)

denoted as M-MTC), the predominant stoichiometries were  $\text{M}_8$ -MTC and  $\text{M}_{12}$ -MTC. Since the Cu(I)-thiolate bonds, unlike Zn(II)-thiolate bonds, persist at low pH, the ESI-MS analysis of a sample containing mainly  $\text{M}_{12}$ -MTC species was carried out under acidic conditions. The results showed the presence of  $\text{Cu}_8$ -MTC, consistent with an initial metal stoichiometry of  $\text{Cu}_8\text{Zn}_4$ -MTC. Considering the metal-binding stoichiometries and the presence of 21 Cys in MTC, a cluster structure in both heterometallic and homometallic forms exists. The CD spectra of both forms are presented in Fig. 4. In these spectra, the CD features above 250 nm originate from the CysS-Cu(I) LMCT transitions. Comparison of the CD intensities of the  $\text{Cu}_8$ -MTC and  $\text{Cu}_8\text{Zn}_4$ -MTC complexes reveals a substantially higher intensity for the heterometallic form, indicating that a mixed Cu(I),Zn(II) cluster(s) was formed. Formation of the new  $\text{Cu}_8\text{Zn}_4$ -MTC species was confirmed by comparing the CD spectrum with the CD spectra of  $\text{Cu}_8$ -MTC and  $\text{Zn}_6$ -MTC, the latter also included in Fig. 4. Within this context it may be noted that MTC isolated from blue crab exposed to copper and cadmium simultaneously yielded heterometallic Cu,Cd-MTC, even though the synthesis of MTC is specifically induced by copper ions [25].

Similar isolation of either homometallic or heterometallic MT species has already been reported and the degree of oxygenation and culture scale have been described as important factors for this behavior [26, 27]. In our case, we obtained these species in multiple syntheses always performed in 2-l Erlenmeyer flasks and under apparently identical oxygenation conditions. We suggest therefore that the high Cys content of these proteins, the ease of their oxidation, the complexity of metal metabolism in bacteria, and/or deficient glutathione content inside the cells may account for these findings. Overall, consistent with the 21 Cys residues in MTC, the copper content in the homometallic  $\text{Cu}_x$ -MTC ( $x = 12$ –14) is higher than that observed for other crustacean MTs containing 18 Cys, where  $x = 10$  [28]. Since the affinity of thiolates for Cu(I) normally tends

to exceed that for Zn(II), the observed formation of heterometallic  $\text{Cu}_x\text{Zn}_y\text{-MTC}$  species in our expression experiments suggests that MTC may be involved in the regulation of both metal ions.

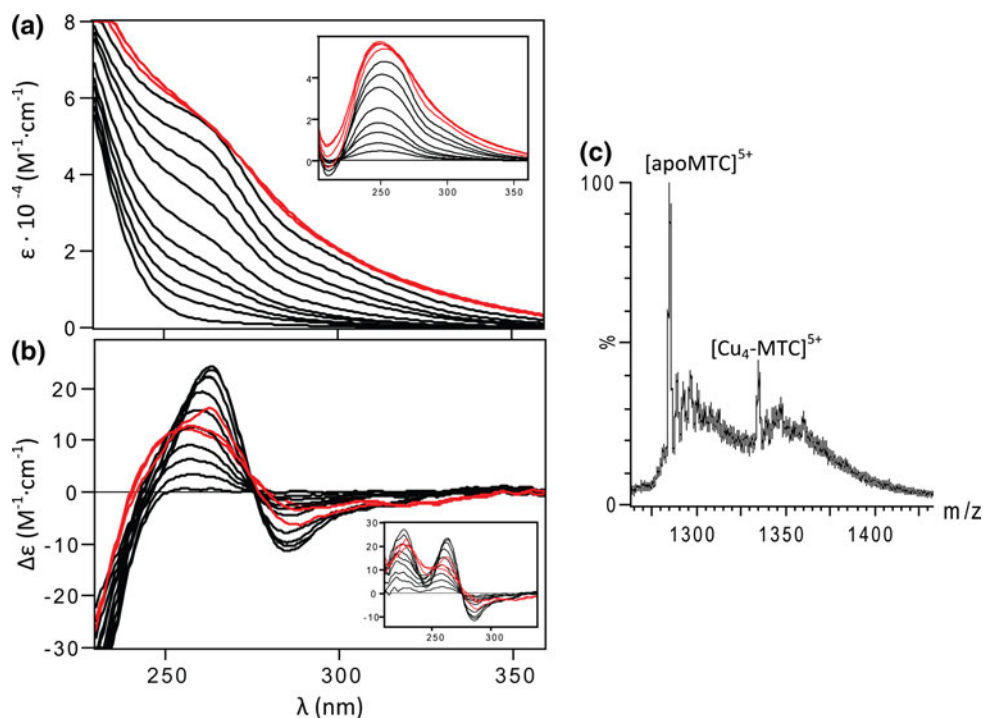
### Cu(I) binding to apoMTC

To gain deeper insight into the formation of homometallic  $\text{Cu}_x\text{-MTC}$  and heterometallic  $\text{Cu}_x\text{Zn}_y\text{-MTC}$  complexes, the filling-up process of apoMTC by Cu(I) and its binding to  $\text{Zn}_{6-8}\text{-MTC}$  were monitored through UV, CD, and ESI-MS measurements. In contrast to the tetrahedral tetrathiolate coordination of Zn(II) ions, the coordination chemistry of Cu(I) thiolates is complex. This is reflected by the diverse coordination geometries of Cu(I) complexes, i.e., digonal, trigonal, and tetrahedral, the coexistence of these binding modes in the same polynuclear complex, and the various ligation modes of thiolate ligands [1, 29]. The only X-ray structure reported for a Cu–MT is that of copper thionein,  $\text{Cu}_8\text{-MT}$ , from yeast. In this structure two copper ions are coordinated digonally and the remaining six trigonally through Cys ligands [30]. Although a number of studies of Cu(I) binding to mammalian MTs have been reported, similar studies of Cu(I) binding to crustacean MTs are lacking. The high susceptibility of Cys ligands to oxidation, particularly significant in nonmammalian MT forms, has been reported as the reason for observing variability in the nuclearity of the Cu(I)–MT complexes [31]. Moreover, unlike zinc- and cadmium-containing MTs, analysis of the ESI-MS data of Cu–MT samples is not

straightforward, mainly owing to the poor ionization of copper-containing species [32].

The UV, CD, and ESI-MS spectra of the titration of apoMTC with Cu(I) are presented in Fig. 5. The absorption spectra developing with increasing Cu(I) concentrations are characterized by a prominent shoulder at 260 nm and a less pronounced shoulder at about 300 nm. These spectral features increase more or less linearly in intensity with the first 9 mol equiv of Cu(I). Moreover, no further changes in intensity were observed with up to 12 Cu(I) (Fig. 5a). As these absorption features originate from the CysS–Cu(I) LMCT transitions [32–35], this behavior indicates that all Cys ligands participate in the binding of nine Cu(I). In the corresponding CD studies, well-resolved CD bands at about (+)260 nm and (–)285 nm were discerned, whose intensity increases almost linearly with the first 8 mol equiv of Cu(I) added (Fig. 5b). Further additions of up to 12 mol equiv of Cu(I) result in a gradual intensity decrease of the overall CD profile. These results together with the absorption data suggest that a well-defined cluster(s) is formed with the first eight or nine Cu(I) and that the binding of about the last four Cu(I) ions results in a rearrangement of the original cluster structure leading to the formation of the  $\text{Cu}_{12}\text{-MTC}$  species. The ESI-MS analyses revealed that upon the addition of the first 2 mol equiv of Cu(I) a  $\text{Cu}_4\text{-MTC}$  complex is formed cooperatively, i.e., in an all-or-nothing process (Fig. 5c). The formation of  $\text{Cu}_4\text{-MTC}$  may be relevant for the development of a higher nuclearity species as already reported for other MTs [32–35]. From this titration point on, the coexistence of

**Fig. 5** ApoMTC titration with copper: **a** electronic absorption and **b** CD spectra of apoMTC after addition of 0–9 mol equiv of Cu(I) (black line) and up to 12 mol equiv of Cu(I) (red line); **c** ESI-MS spectra after addition of 2 mol equiv of Cu(I). *Insets:* The family of corresponding difference spectra obtained by subtracting the spectrum of apoMTC from spectra recorded after  $n$  mol equiv of Cu(I) had been added ( $n = 1\text{--}12$ )



several Cu–MTC species is a common feature in all titration steps. Among the various stoichiometries observed in ESI-MS, Cu<sub>6</sub>–MTC, Cu<sub>8</sub>–MTC, Cu<sub>10</sub>–MTC, and Cu<sub>12</sub>–MTC appear to be predominant (data not shown). The observation of the latter forms points to equilibrium processes not seen in the CD and UV studies. However, as ESI-MS is not a quantitative method and in view of the difficulties in acquiring the ESI-MS data on Cu(I)–MT complexes, how much these data represent the situation in aqueous solution is not clear.

To gain insight into the heterometallic Cu<sub>x</sub>Zn<sub>y</sub>–MTC species formed in the recombinant synthesis, the titration of Zn<sub>6–8</sub>–MTC with Cu(I) at pH 7 was carried out, monitoring the spectral features of the CysS–Cu(I) LMCT bands (Fig. 6). Although the developing absorption and CD profiles upon the addition of Cu(I) to Zn<sub>6–8</sub>–MTC were similar to those obtained in the Cu(I) titration of apoMTC

(Fig. 5), in the former case the maximum intensity was reached with 12 to 13 Cu(I) and in the latter with eight to nine Cu(I) added. This suggests that the Cu(I) binding to the preformed structure of Zn<sub>6–8</sub>–MTC differs from that of apoMTC. To investigate whether the heterometallic Cu<sub>x</sub>Zn<sub>y</sub>–MTC species obtained by displacement of Zn(II) during the titration of Zn<sub>6–8</sub>–MTC by Cu(I) and those obtained by recombinant biosynthesis are structurally similar, the intensity of the corresponding CD profiles were compared. Regardless of the metal stoichiometries in Cu<sub>x</sub>Zn<sub>y</sub>–MTC complexes generated in vitro, their CD intensity was always more than 50% lower than that of the biosynthetic Cu<sub>8</sub>Zn<sub>4</sub>–MTC (Fig. 6c). This finding indicates that a different folding pathway for the formation of the heterometallic species in vivo and in vitro exists. Concerning the former, the prokaryotic organism *E. coli* is considered as a good alternative to obtain the native MT protein [36]. The observed structural differences imply that the in vivo metallation process does not proceed by a prior incorporation of Zn(II) into the nascent protein followed by its displacement by Cu(I). This hypothesis is supported by the observation made in crab hepatopancreas tissue explants exposed to copper, where copper binding directly to newly synthesized MT has been described [16].

#### Characterization of reconstituted Cd<sub>8</sub>–MTC

Because Zn(II) is a *d*<sup>10</sup> metal with no outer-shell unpaired electrons, it is spectroscopically silent. The coordination environment of Zn(II) sites in proteins and their organization are often probed with <sup>113</sup>Cd(II), which possesses the nuclear spin 1/2. To aid our <sup>113</sup>Cd NMR studies, the reconstituted Cd–MTC form was generated and characterized by the standard technique already applied to the Zn(II)-containing MTC form (Table 2). The ICP-AES and ESI-MS characterization of the product showed the presence of only one species, Cd<sub>8</sub>–MTC, with a high degree of purity (protein content in reduced form of 95%). The electronic absorption and CD spectra of Cd<sub>8</sub>–MTC are presented in Fig. 7. The absorption spectrum is characterized by a typical metal-induced shoulder at 250 nm, observed in all Cd–MTs and originating from CysS–Cd(II) LMCT transitions, with the molar extinction coefficient within the range (1.0–1.1) × 10<sup>5</sup> M<sup>−1</sup> cm<sup>−1</sup>. As the absorbance of a single Cd–S bond is about 5,000 M<sup>−1</sup> cm<sup>−1</sup> [37], this indicates that all 21 Cys are involved in metal binding. This conclusion is supported by the titration of apoMTC with Cd(II) (Fig. 8), where a developed plateau with more than eight Cd(II) added shows the same molar absorptivity. The corresponding CD profile of Cd<sub>8</sub>–MTC is characterized by two broad positive features, a band at (+)255 nm and a shoulder at (+)235 nm. This CD profile differs substantially from the CD profiles reported for mammalian and crustacean

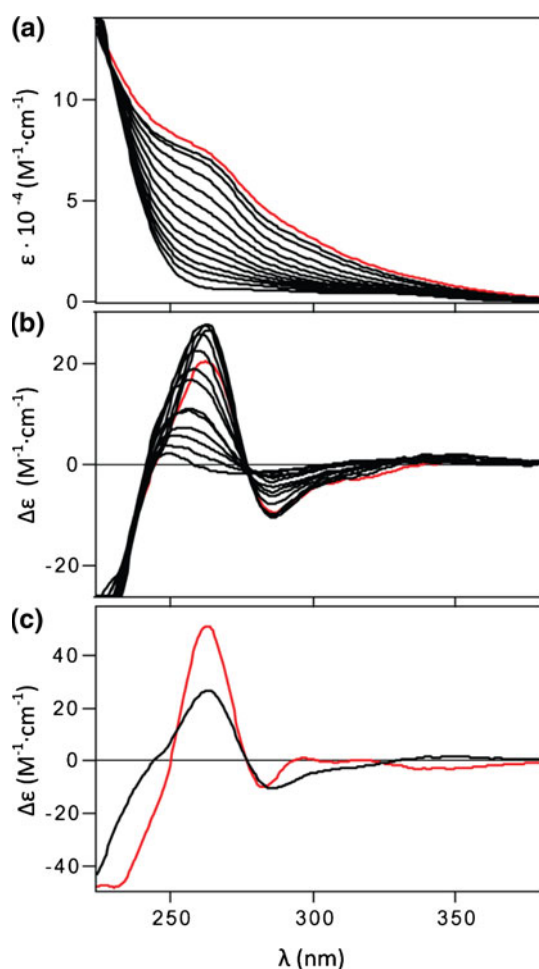


**Fig. 6** **a** Electronic absorption and **b** CD spectra of the Zn<sub>6–8</sub>–MTC titration with copper at pH 7 after addition of 0–12 mol equiv of Cu(I) (black line) and 13 mol equiv of Cu(I) (red line); **c** comparison of the most chiral CD (black line) spectrum obtained in the titration [after addition of 12 mol equiv of Cu(I)] with that of the biosynthetic Cu<sub>8</sub>Zn<sub>4</sub>–MTC species (red line)



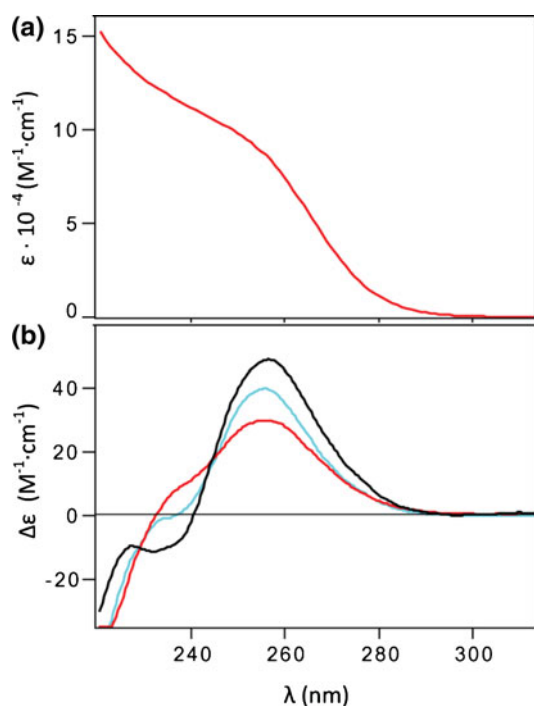


**Fig. 7** **a** Electronic absorption and **b** CD spectra of reconstituted  $\text{Cd}_8\text{-MTC}$  (red line). Consistent with ESI-MS data (Table 2), treatment of the latter species with Chelex 100 showed after a few minutes the presence of a mixture of  $\text{Cd}_7\text{-MTC}$  and  $\text{Cd}_8\text{-MTC}$  (blue line), which after 2–3 h evolved into  $\text{Cd}_7\text{-MTC}$  exclusively (black line)

$\text{Cd-MTs}$  [18, 23, 38], where maxima at about (+)260, (–)240, and (+)228 nm have been discerned. In these MTs, the oppositely signed low-energy CD bands at (+)260 and (–)240 nm have been assigned to the excitonically coupled transition dipole moments of the bridging thiolate ligands within the cluster structure. Thus, in  $\text{Cd}_8\text{-MTC}$  the biphasic CD profile, often used as a fingerprint of a cluster structure, is not observed, implying unfavorable cluster geometry for such a coupling. That a cluster structure also exists in  $\text{Cd}_8\text{-MTC}$ , albeit with an unusual cluster geometry, is evidenced from both the stoichiometry of Cys/Cd of 2.62 in  $\text{Cd}_8\text{-MTC}$  and the position of the low-energy CD band at (+)255 nm, diagnostic of the presence of bridging thiolate ligands.

To examine whether the fully cadmium loaded  $\text{Cd}_8\text{-MTC}$  possesses metal binding sites of different affinity, as already observed for the  $\text{Zn(II)}$  ions, this form was treated with Chelex 100 resin and characterized by CD (Fig. 7) and ESI-MS (Table 2). Combination of both sets of data shows that a new  $\text{Cd}_7\text{-MTC}$  species was formed. Remarkably, the CD envelope of  $\text{Cd}_7\text{-MTC}$  shows a biphasic profile with maxima at (+)258 and (–)235 nm, comparable to that found in other  $\text{Cd-MT}$  species [18, 23, 38, 39], and an increased intensity when compared with  $\text{Cd}_8\text{-MTC}$ . These data indicate that the Chelex 100 treatment not only causes the release of one more loosely bound

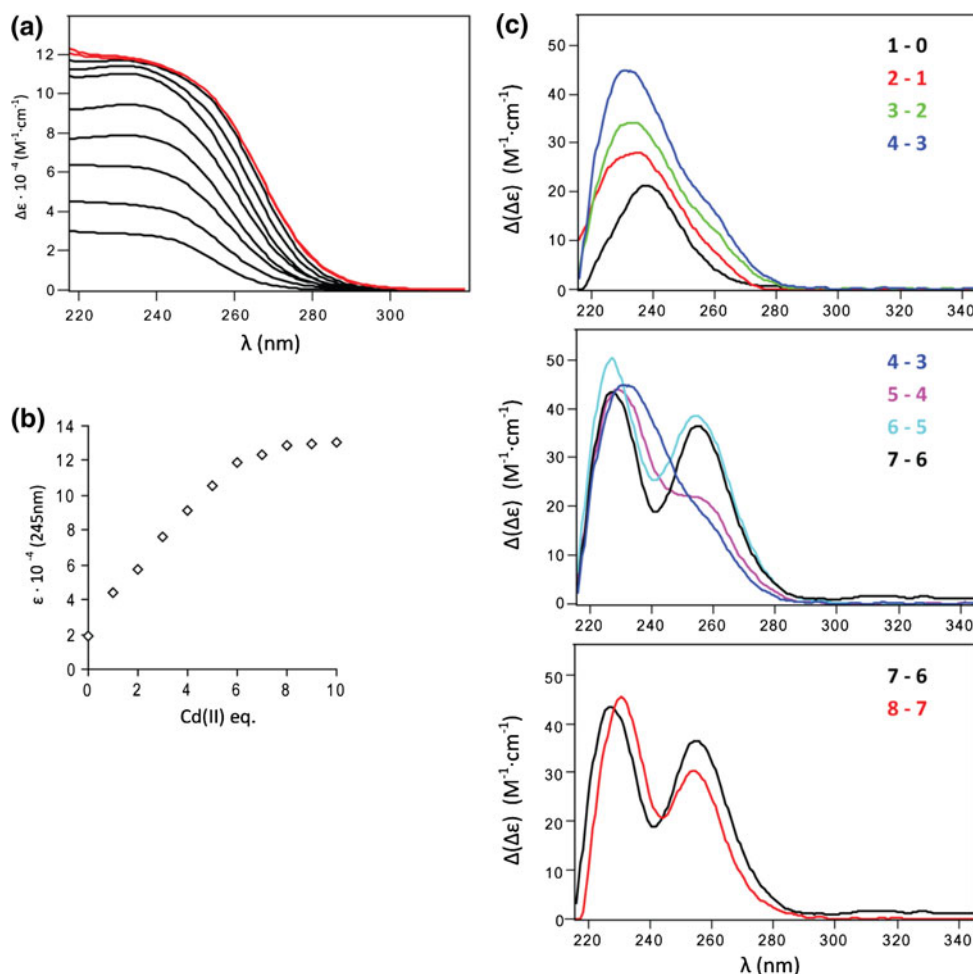
$\text{Cd(II)}$  ion, but also leads to changes in the protein structure. Similarly to the reversible interconversion observed between  $\text{Zn}_6\text{-MTC}$  and  $\text{Zn}_8\text{-MTC}$ , the addition of 1 mol equiv of  $\text{Cd(II)}$  to  $\text{Cd}_7\text{-MTC}$  yielded  $\text{Cd}_8\text{-MTC}$ . To investigate the involvement of free Cys residues in the interconversion process between  $\text{Cd}_8\text{-MTC}$  and  $\text{Cd}_7\text{-MTC}$ , the latter species was titrated with NaOH up to pH 11. Unlike the UV titration of  $\text{Zn}_6\text{-MTC}$ , in this case only a very small increase of absorbance at 237 nm was observed, suggesting that  $\text{Cd}_7\text{-MTC}$  has at most one free Cys able to participate in the binding of the eighth  $\text{Cd(II)}$  ion (data not shown). Comparison of the stoichiometry of the  $\text{M(II)-MTC}$  species obtained by reconstitution of apoMTC ( $\text{Zn}_{6-8}$  vs.  $\text{Cd}_8$ ) and after Chelex 100 treatment ( $\text{Zn}_6$  vs.  $\text{Cd}_7$ ) shows that although MTC possesses two binding sites with different affinity toward both  $\text{Zn(II)}$  and  $\text{Cd(II)}$ , the final metal stoichiometries differ.

pH-titration studies were carried out to study the stability of the cluster structure in  $\text{Cd}_8\text{-MTC}$ . The displacement of  $\text{Cd(II)}$  by competition with increasing concentrations of protons in the medium was followed by the changes in the cadmium-induced shoulder at 250 nm in the absorption spectra [40]. The graphical representation of the degree of  $\text{Cd(II)}$  release with progressive acidification of  $\text{Cd}_8\text{-MTC}$  as a function of pH is indicative of a two-step process (Fig. S2). In the first step, only one  $\text{Cd(II)}$  ion is released within the pH range 6–4, whereas in the second step, the remaining seven  $\text{Cd(II)}$  ions are released within the narrow pH range between 4 and 3. Since the titration curve did not display a pronounced two-step titration profile, only the overall apparent binding constant was calculated. The apparent binding constant at pH 7 of  $K_{\text{app}} = 3 \times 10^{14} \text{ M}^{-1}$  obtained is similar to the apparent binding constants reported previously for a number of other  $\text{Cd-MTs}$  from various species using the same method [41, 42]. The calculation of the apparent stability constant is described in “Materials and methods” and is based on the following premises: (1) in  $\text{Cd}_8\text{-MTC}$  all 21 Cys participate in metal binding, yielding the molar ratio of Cys to cadmium of 2.62; (2) the pH midpoint value found for the whole titration is 3.28 (Fig. S2). From the removal of the eighth  $\text{Cd(II)}$  by Chelex100, it can be concluded that its apparent stability constant must be lower than that of the  $\text{Cd(II)-Chelex100}$  complex, which was estimated to be approximately  $10^{4.6} \text{ M}^{-1}$  [39].

#### Binding of $\text{Cd(II)}$ to apoMTC

To learn more about the formation of the  $\text{Cd}_8\text{-MTC}$  complex, the stepwise binding of  $\text{Cd(II)}$  to apoMTC was monitored through UV, CD, and ESI-MS measurements. To ensure strict oxygen-free conditions, independent samples were prepared for each titration point (see

**Fig. 8** ApoMTC titration with Cd(II). **a** UV difference spectra, Cd-MTC versus apoMTC, obtained after addition of 1–10 mol equiv of Cd(II). The spectra obtained after addition of 9 and 10 mol equiv of Cd(II), depicted in *red lines*, are nearly coincident. **b** Molar extinction coefficient at 245 nm against the number of mole equivalents of Cd(II) added. **c** CD difference spectra, CdMTC versus apoMTC, after addition of 1–8 mol equiv of Cd(II).



“Materials and methods”). The results obtained on samples adjusted to pH 7.2 are presented in Fig. 8.

The difference absorption spectra of Cd-MTC versus apoMTC show an incremental increase of a metal-induced shoulder at 245 nm with the first about 4 mol equiv of Cd(II) ( $\Delta\epsilon$  is approximately  $72,000 \text{ M}^{-1} \text{ cm}^{-1}$ ) (Fig. 8a, b). Further increase in absorption with the next 2 mol equiv of Cd(II) ( $\Delta\epsilon$  is approximately  $28,000 \text{ M}^{-1} \text{ cm}^{-1}$ ) was accompanied by a small redshift to about 250 nm. The binding of the last 2 mol equiv of Cd(II) is characterized by a substantial redshift of the absorption envelope to about 262 nm and only a small intensity increase ( $\Delta\epsilon$  is approximately  $9,000 \text{ M}^{-1} \text{ cm}^{-1}$ ) (Fig. 8a). In the corresponding CD studies (Fig. 8c), the binding of the first 4 mol equiv of Cd(II) induces an incremental increase of a broad positive CD band centered at 240 nm with a weak shoulder at about 250 nm, a feature resembling that seen in the absorption spectra. Upon the addition of the fifth and sixth Cd(II), mainly a strong CD band at (+)250 nm develops. This CD profile is almost unaffected by the binding of the last two Cd(II) (Fig. 8c). The ESI-MS characterization of the metal binding process revealed at each titration point the predominance of the Cd-MTC

complexes containing the number of Cd(II) mole equivalents added. This indicates that the formation of  $\text{Cd}_8\text{-MTC}$  is a noncooperative process (Fig. S3). Taking into account that in the absorption spectra of Cd-MTs the first CysS–Cd(II) LMCT transition of bridging thiolates occurs at 250 nm and that the transformation of the original terminal to bridging thiolates is accompanied by a 6-nm redshift [43], the observed development of the absorption and CD features suggests the following binding process. The spectral features occurring at about 240–245 nm in both the absorption and the CD spectra with the first four Cd(II) would be consistent with the preferential formation of independent Cd(II) sites. This is supported by the molar absorptivity obtained for the initial  $\text{Cd}_4\text{-MTC}$  complex, which, when divided by the reported molar absorptivity of a single Cd–S bond of  $5,000 \text{ M}^{-1} \text{ cm}^{-1}$  [37], corresponds to about 14 thiolate ligands. This result is in line with the tetrathiolate metal coordination by mainly terminal thiolate ligands. In the next binding step, the redshift and the involvement of about six Cys in the binding of two additional Cd(II) suggest that in the  $\text{Cd}_6\text{-MTC}$  complex a cluster structure is formed, which is almost unperturbed by the binding of the last two Cd(II) ions. In the latter case,

only about one or two Cys ligands would participate in their binding. However, the occurrence of a dramatic red-shift of the absorption envelope suggests that a transformation of a significant number of originally terminal thiolates to bridging thiolates must occur. We suggest, therefore, that the last two Cd(II) would just expand the original cluster structure(s) in Cd<sub>6</sub>-MTC. Such behavior is unique to MTC, as it was not seen in similar studies of MTs from various species.

#### <sup>1</sup>H and <sup>113</sup>Cd NMR studies of Cd<sub>7</sub>-MTC

Several <sup>113</sup>Cd<sub>7</sub>-MTC samples were used to perform the NMR experiments. In the sample preparations, their concentration to up to 1 mM usually produced protein aggregates, precipitates, loss of metal ions, or a combination thereof. We found that the presence of β-mercaptoethanol (β-MeSH) was useful in avoiding the sample degradation. However, the presence of this reducing agent in samples is accompanied with difficulties in obtaining a full set of NMR data required for structural studies. β-MeSH contains protons with chemical shifts between 3.0 and 3.5 ppm, overlapping with the β-protons of Cys residues and at high concentrations hampers 2D homonuclear <sup>1</sup>H NMR experiments necessary to obtain the sequence specific assignment of amino acids. Therefore, two sets of NMR-acceptable samples were generated. The first, designated MTC(1), contained a relatively low concentration of β-MeSH (0.5–1 mM) and was used for both <sup>1</sup>H and <sup>113</sup>Cd NMR experiments. The second, designated MTC(2), contained a high concentration of β-MeSH (10–30 mM). However, owing to the presence of intense proton signals of β-MeSH at about 3.50 ppm, this sample was not suitable for 2D <sup>1</sup>H NMR experiments. In this case, only the 1D <sup>113</sup>Cd and heteronuclear <sup>1</sup>H–<sup>113</sup>Cd NMR experiments were successful.

<sup>113</sup>Cd direct acquisition spectra for samples <sup>113</sup>Cd<sub>7</sub>-MTC(1) and <sup>113</sup>Cd<sub>7</sub>-MTC(2) are shown in Fig. 9a. MTC(1) and MTC(2) display three and seven well-resolved <sup>113</sup>Cd signals, respectively. The chemical shift position of these resonances occurs between 590 and 700 ppm (Table 3) and is thus closely similar to that observed in <sup>113</sup>Cd NMR studies of other Cd-MTs. This suggests that in <sup>113</sup>Cd<sub>7</sub>-MTC the metal coordination by both terminal and bridging thiolate ligands is present. The <sup>1</sup>H–<sup>113</sup>Cd heteronuclear multiple quantum correlation (HMQC) spectra show correlations between the <sup>113</sup>Cd metal ions and the β-protons of Cys residues bound to them (Fig. 9b). The chemical shift position of the <sup>113</sup>Cd signals (A1–A3) in the <sup>1</sup>H–<sup>113</sup>Cd HMQC spectrum of MTC(1) (Fig. 9b, red) is identical to that observed in the <sup>113</sup>Cd direct acquisition spectrum, indicating that the three <sup>113</sup>Cd ions are bound to the polypeptide chain through Cys thiolates. In the

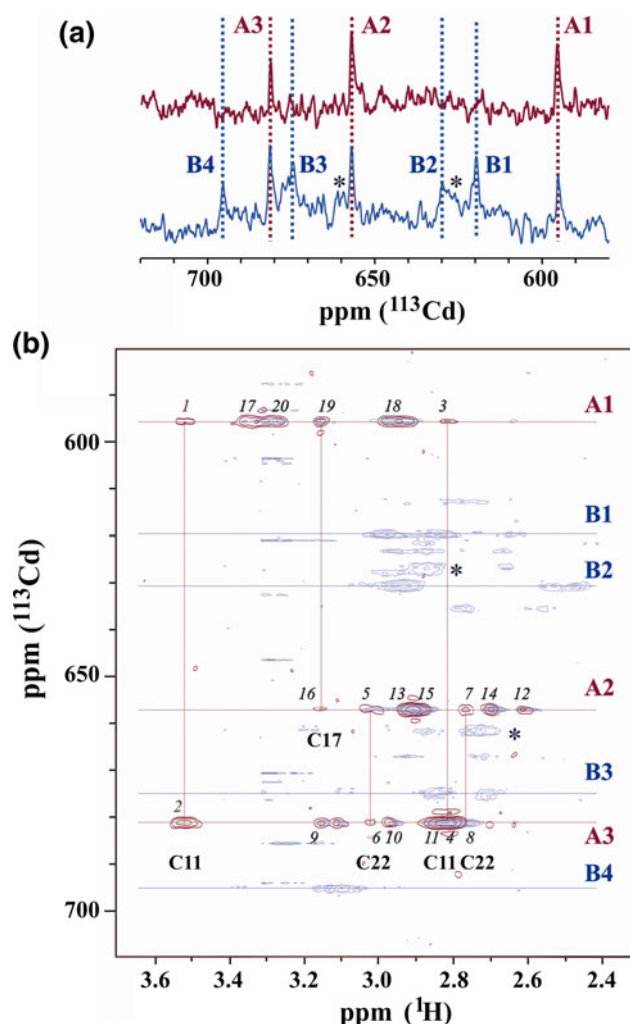


**Fig. 9** **a** <sup>113</sup>Cd NMR spectrum of MTC(1) (red) and MTC(2) (blue) samples. Signals A1–A3 (numbered according to their chemical shifts) are observed in both samples, whereas signals B1–B4 are exclusive of MTC(2). **b** Superposition of <sup>1</sup>H–<sup>113</sup>Cd heteronuclear multiple quantum correlation spectra of MTC(1) (red) and MTC(2) (blue). A1–A3 and B1–B4 <sup>113</sup>Cd signals are labeled with horizontal dashed lines. Cross-peaks from cluster A signals are numbered in *italics* (see the text). Vertical dashed lines correspond to protons belonging to Cys bridges. Signals with lower intensity are marked with asterisks in both spectra

<sup>1</sup>H–<sup>113</sup>Cd HMQC spectrum of MTC(2) (Fig. 9b, blue), seven clearly defined <sup>113</sup>Cd signals are observed, of which three (A1–A3) have the same <sup>1</sup>H and <sup>113</sup>Cd chemical shifts observed in MTC(1) samples (Fig. 9b, red); the other four resonances (B1–B4) show completely different chemical shifts with respect to MTC(1) for both types of nuclei.

Standard 2D homonuclear <sup>1</sup>H NMR experiments were carried out on <sup>113</sup>Cd<sub>7</sub>-MTC(1). Attempts to perform analogous experiments with <sup>113</sup>Cd<sub>7</sub>-MTC(2) were unsuccessful owing to the high concentration of β-MeSH present in these samples (see above). The reconstituted <sup>113</sup>Cd<sub>7</sub>-MTC contains 66 amino acids, including 64 from the native MTC form and two from the Gly-Ser peptide introduced at

**Table 3**  $^{113}\text{Cd}$  and  $^1\text{H}$  chemical shifts for MTC(1) and MTC(2) samples obtained from  $^{113}\text{Cd}$  direct and  $^1\text{H}$ – $^{113}\text{Cd}$  heteronuclear multiple quantum correlation experiments

Cluster	Cd signal	Observed cross peaks <sup>a</sup> (ppm)		Cys number
		$^{113}\text{Cd}$	$^1\text{H}^b$	
A (N-terminus)	A1 (Cd1)	681.5	3.34 (17), 2.95 (18)	Cys3
			3.15 (19)	Cys17 <sup>c</sup> (bridge with A2)
			3.52 (1), 2.82 (3)	Cys11 (bridge with A3)
			3.29 (20)	Cys18 <sup>c</sup> or Cys24 <sup>c</sup>
	A2 (Cd2)	656.8	3.15 (16)	Cys17 <sup>c</sup> (bridge with A1)
			2.89 (15), 2.70 (14)	Cys16
			2.99 (5), 2.76 (7)	Cys22 <sup>c</sup> (bridge with A3)
			2.91 (13), 2.61 (12)	Cys27
	A3 (Cd3)	594.7	3.14 (9)	Cys5 <sup>c</sup>
			2.94 (10), 2.83 (11)	Cys9
			3.52 (2), 2.82 (4)	Cys11 (bridge with A1)
			2.99 (6), 2.76 (8)	Cys22 <sup>c</sup> (bridge with A2)
B (C-terminus)	B1	619.5		
	B2	630.0		
	B3	675.6		
	B4	696.8		

<sup>a</sup> Since only cluster A (N-terminus) has been sequentially assigned, only the cross-peaks corresponding to this cluster are shown

<sup>b</sup> The numbers in *parentheses* correspond to the cross-peaks cited in the text and shown in Fig. 9

<sup>c</sup> Tentative assignment (see the text)

the N-terminus by the cloning strategy (see above). As four of them are Pro residues, a total of 61 amide protons are expected to be observed in the fingerprint region of the 2D homonuclear  $^1\text{H}$  spectra. However, of these 61 amide protons only 30 amide protons (49.2%) were detected in the 2D spectra of MTC(1) (see the nuclear Overhauser enhancement spectroscopy spectrum in Fig. S4). Therefore, only the sequence-specific assignment of the spin systems attached to these amide protons was carried out (Table S2). The assignment includes, besides the attached residue Ser, residues 1–31 of MTC, with the exception of amino acids 2 and 28, which are Pro residues. Since amide protons corresponding to amino acids 32–64 could not be detected, it would appear that the first 31 amino acids of MTC(1) give rise to the N-terminal domain of MTC (see below).

With the sequence-specific assignment at hand (Table S2), the analysis of the  $^1\text{H}$ – $^{113}\text{Cd}$  HMQC spectrum of  $^{113}\text{Cd}_7$ –MTC(1) was carried out (Fig. 9b). The analysis provides information as to the sequence-specific connectivities between the  $\beta$ -protons of Cys and  $^{113}\text{Cd}$  (resonances A1–A3) and thus the organization of the three Cd(II) sites. Attempts to perform other heteronuclear experiments, correlating through more bonds of the Cys side chains, were unsuccessful owing to the relatively low concentration of the samples for these less-sensitive experiments and mainly to a large line broadening of the  $^1\text{H}$  and  $^{113}\text{Cd}$  resonances. The results provide evidence for

the existence of a three-metal cluster in  $^{113}\text{Cd}_7$ –MTC(1). A scheme of the connectivities present in the N-terminal cluster of MTC is shown in Fig. 10. The following assignment was performed by comparing the  $^1\text{H}$  chemical shifts of  $\beta$ -protons of the specifically assigned Cys ligands found in the homonuclear experiments (Table S2) with those observed in the heteronuclear experiments (Table 3).

In the heteronuclear spectra both Cd1 and Cd3 ions give cross-peaks with a  $\beta$ -proton at 3.52 ppm (cross-peaks 1 and 2 in Fig. 9b), which unequivocally belongs to

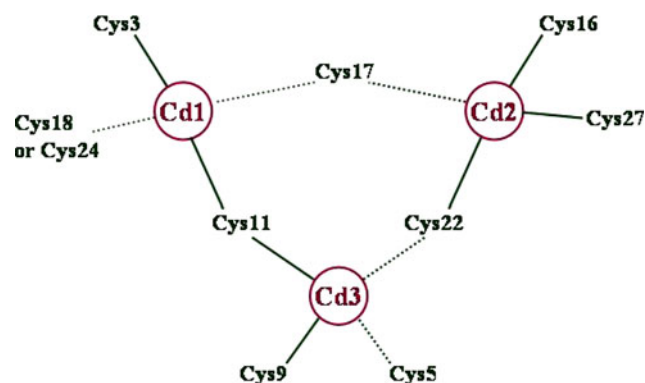


**Fig. 10** Cadmium to Cys connectivities found in the N-terminal domain (cluster A) of MTC on the basis of NMR data. *Dashed lines* indicate tentative connectivities. Cadmium numeration corresponds to the chemical shifts (signals A1–A3 in Fig. 9)



bridging Cys11 as the cross-peaks with the other geminal proton at 2.82 ppm (cross-peaks 3 and 4) were also identified (Table 3). Likewise, the Cd2 and Cd3 ions show weak, but resolved cross-peaks at 2.99 ppm (cross-peaks 5 and 6) that correspond to one  $\beta$ -proton of Cys22. Cross-peaks between a signal at 2.76 ppm and Cd2 (cross-peak 7) confirm the coordination of this cadmium ion to this Cys. The equivalent cross-peak with Cd3 (cross-peak 8) is probably also present, although in an overlapping region of several Cys  $\beta$ -protons. Consequently, Cys22 is the most probable candidate to link these two metal ions. One well-resolved cross peak at 3.14 ppm (cross-peak 9) is observed for the Cd3 ion. This peak can exclusively arise from Cys5 or Cys17. The  $\beta$ -proton partner of either of these Cys residues does not allow us to discriminate between these two possibilities. The  $^{113}\text{Cd}$  signal A3 also provides a heteronuclear correlation with proton resonances at 2.94 ppm (cross-peak 10) and 2.83 ppm (cross-peak 11), corresponding to the  $\beta$ -protons of Cys9. Thus, we tentatively propose that the Cd3 ion is bound to Cys9, Cys11 (bridging Cd1), Cys22 (bridging Cd2), and either Cys5 or Cys17. For the Cd2 ion resolved cross-peaks are observed between the  $^{113}\text{Cd}$  signal A2 and protons with chemical shift at 2.61 ppm (cross-peak 12) and 2.91 ppm (cross-peak 13), unequivocally corresponding to the  $\beta$ -protons of Cys27. The A2 signal of Cd2 ion is also scalar-connected to  $\beta$ -protons of Cys residues with chemical shifts at 2.70 ppm (cross-peak 14) and 2.89 ppm (cross-peak 15) (Cys16). A very weak, but resolved, cross-peak between the A2 signal and a  $\beta$ -proton at 3.15 ppm (cross-peak 16) could correlate this metal ion with either Cys 5 or Cys17. Thus, the Cd2 ion is probably bound to Cys16, Cys22 (bridging Cd3), Cys27, and either Cys5 or Cys17.

Cross-peaks related to the Cd1 ion are even more difficult to assign. Two cross-peaks between the  $^{113}\text{Cd}$  signal A1 and the Cys  $\beta$ -protons at 3.34 ppm (cross-peak 17) and 2.95 ppm (cross-peak 18) correspond to Cys3. The presence of a cross-peak at 3.15 ppm (cross-peak 19) suggests that either Cys5 or Cys17 may also be involved in the binding of Cd1, forming then the bridge between Cd1 and Cd2. Its geminal partner, however, does not produce any cross-peaks. The additional A1 cross-peak at 3.29 ppm (cross-peak 20) could correspond to either Cys18 or Cys24. Overall, the Cd1 ion is coordinated with Cys3 and Cys11 (bridge with Cd3) and with either Cys5 or Cys17 (then, one of these two Cys would act as a bridge with Cd2). It is remarkable that Cys17 forms part of the first Cys triplet, i.e., Cys16–Cys17–Cys18.

In all Cys doublets present in MTs, one of the Cys residues is bound to a metal ion as a terminal ligand and the other Cys bridges this metal ion to a second one [2, 14, 15]. Since Cys16 is bound to Cd2, the previously

cited ambiguity between Cys5 or Cys17 can be resolved in favor of the latter. In other words, we can tentatively assign Cys17 as the bridging ligand between Cd1 and Cd2 ions. Consequently, Cys5 would be the fourth ligand of Cd3. The inspection of available MT structures reveals the following metal-binding properties of Cys ligands in the structural motifs Cys-X-Cys (where X is an amino acid different from Cys), Cys-Cys, and Cys-Cys-Cys. In the Cys-X-Cys sequences both Cys can act as terminal ligands, terminal and bridging ligands, but not as bridging ligands only. In the Cys-Cys and Cys-Cys-Cys sequences the first N-terminal Cys is always a terminal ligand and the second one is a bridging ligand and, on the basis of our studies, the last Cys in the Cys triplet is a terminal ligand.

So far the 3D structure of crustacean MTs is only known for the crab *H. americanus* [15] and *C. sapidus* MT-1 [14], both consisting of the two  $\text{M}_3^{113}\text{Cys}_9$  clusters. The N-terminal cluster is generally denoted as  $\beta_{\text{N}}$  and the C-terminal cluster as  $\beta_{\text{C}}$ . According to the alignment of the primary sequences (Fig. 1), we assume that the N-terminal domain in MTC contains a similar number of amino acid residues as the  $\beta_{\text{N}}$  domain in the two already determined structures. This provides independent support for the presence of a two-domain structure in MTC, with the N-terminal domain containing 31 amino acids. However, none of the 33 C-terminal amino acids are observed in homonuclear experiments of MTC(1). In this sample, prepared at a low  $\beta$ -MeSH concentration, exchange phenomena are likely to occur in the second cluster, and so neither Cd(II) ions nor amide protons are observed in the respective experiments. Note also that  $^{113}\text{Cd}_7\text{-MTC}$  was generated from  $^{113}\text{Cd}_8\text{-MTC}$  through the removal of one more labile Cd(II) by Chelex 100. However, the rate of chemical exchange is clearly affected by the presence of a high  $\beta$ -MeSH concentration since seven  $^{113}\text{Cd}$  resonances were detected in the direct acquisition spectra of  $^{113}\text{Cd}_7\text{-MTC}(2)$ . These results suggest that the C-terminal domain of MTC contains 33 amino acid residues and binds four Cd(II) ions. Furthermore, the chemical shift position of the corresponding four  $^{113}\text{Cd}$  resonances (B1–B4) is consistent with their clustered organization (Fig. 9a). That in our studies both MTC(1) and MTC(2) contained a full complement of seven Cd(II) ions is supported by our observation that when  $^{113}\text{Cd}_7\text{-MTC}(2)$  samples were either passed through a gel filtration column or treated with Centricon devices (to remove  $\beta$ -MeSH), the resulting NMR spectra (either  $^1\text{H}$  or  $^{113}\text{Cd}$  homonuclear, or  $^1\text{H}$ – $^{113}\text{Cd}$  heteronuclear) were essentially identical to those obtained with  $^{113}\text{Cd}_7\text{-MTC}(1)$  samples. In other words, the removal of the reducing agent from MTC(2) produced MTC(1). It is also interesting that some minor  $^{113}\text{Cd}$  signals (marked with an asterisk) are observed in both  $^{113}\text{Cd}$  direct and  $^1\text{H}$ – $^{113}\text{Cd}$  HMQC experiments carried out on the MTC(2) samples

(Fig. 9). Although their origin is not clear, they may originate either from unspecific Cd(II) binding or, more likely, from a subset of cluster structure(s) undergoing exchange processes.

## Conclusions

The present studies on the blue crab copper specific MT MTC with six Cys residues organized in two Cys triplets have afforded so far unobserved metal-binding properties in this class of proteins. We have shown that all 21 Cys residues of MTC participate in the binding of Cu(I), Zn(II), and Cd(II) ions, indicating that also Cys residues of both Cys triplets act as ligands. MTC binds eight divalent Zn(II) or Cd(II) metal ions. Both metalloforms possess high- and low-affinity metal binding sites. Whereas the treatment of Zn<sub>8</sub>-MTC with the complexing resin Chelex 100 removes two Zn(II), only one Cd(II) is removed from Cd<sub>8</sub>-MTC. A possible reason is the difference in the M(II)–S(Cys) bond energy, which follows the order Zn(II) is lower than Cd(II). In contrast to M<sub>8</sub><sup>II</sup>-MTC, the resulting metal-deficient forms Zn<sub>6</sub>-MTC and Cd<sub>7</sub>-MTC contain two and one free Cys, respectively. The NMR characterization of Cd<sub>7</sub>-MTC suggests the presence of a two-domain structure, each domain containing one Cys triplet and encompassing either the three-metal or the four-metal thiolate cluster. The three-metal cluster is located in the N-terminal domain (residues 1–31) and the four-metal cluster in the C-terminal domain (residues 32–64), in which ten and 11 Cys residues are present, respectively. The scheme of the metal–Cys connectivities in the three-metal cluster of Cd<sub>7</sub>-MTC presented resembles that of cyclohexane-like clusters present in a number of MTs. In these clusters six terminal and three bridging Cys ligands are present. Since the metal organization determined in the three-metal cluster reveals a Cd<sub>3</sub>Cys<sub>9</sub> structure, the one free Cys in Cd<sub>7</sub>-MTC must be present in the N-terminal domain, presumably Cys in the triplet. Although the presence of a Cd<sub>3</sub>Cys<sub>9</sub> cluster in the N-terminal domain has been shown, the cluster organization in the C-terminal domain could not be determined owing mainly to chemical exchange processes.

The studies of the filling-up process of apoMTC with Cd(II) ions suggest that the cluster structure develops with the first six Cd(II) added, i.e., Cd<sub>6</sub>-MTC, and that its generation is preceded by the formation of four independent tetrathiolate Cd(II) complexes. The binding of the last two Cd(II) ions, forming Cd<sub>8</sub>-MTC, is associated with the transformation of a large number of originally terminal thiolates to bridging thiolates and almost no changes in the cluster structure of the Cd<sub>6</sub>-MTC complex. These features are unique to MTC and point to the formation of an unusual cluster structure in Cd<sub>6</sub>-MTC. On

the basis of our NMR data, we infer that in Cd<sub>6</sub>-MTC each domain contains a Cd<sub>3</sub>-thiolate cluster. Then, the attractive possibility accounting for the observed absorption and CD features is the scenario in which the last two Cd(II) act as a cap generating the Cd<sub>4</sub>Cys<sub>10</sub> and Cd<sub>4</sub>Cys<sub>11</sub> clusters in the N- and C-terminal domains, respectively. In this respect, the former may resemble an adamantane-like structure and the latter a four-metal cluster found in a number of mammalian Cd<sub>7</sub>-MTs. The characterization of Zn-MTC shows that also in this case the formation of Zn<sub>8</sub>-MTC is preceded by a stabler Zn<sub>6</sub>-MTC form, whose structure is unaffected by the binding of the last two Zn(II). Thus, the intermediate M<sub>6</sub><sup>II</sup>-MTC complex with two metal–thiolate clusters forms a rigid scaffold, owing presumably to the presence of one Cys triplet and two Pro in each protein domain.

In the studies of the stepwise binding of Cu(I) to apo-MTC, the absorption and CD features that developed suggest that all 21 Cys are involved in the binding of eight to nine Cu(I) ions and that the addition of about four Cu(I) results in structural changes of Cu<sub>8–9</sub>-MTC and the formation of Cu<sub>12</sub>-MTC. This is in a marked contrast to similar studies of mammalian MT-1 and MT-3 (20 Cys), where an increase in absorption occurred with up to 12 Cu(I) [34, 35]. In these studies, a digonal and trigonal Cu(I) coordination was suggested. However, the Cu(I)-to-MTC stoichiometry in Cu<sub>8–9</sub>-MTC is similar to that obtained with divalent metal ions. This may suggest that in Cu<sub>8–9</sub>-MTC the Cu(I) ions are organized in two metal–thiolate clusters in which a tetrathiolate Cu(I) coordination exists. Such a Cu(I) coordination has not been reported in other Cu-MTs. In this regard, it should be noted that a direct replacement of Zn(II) from the sites in Zn<sub>6–8</sub>-MTC by Cu(I) did not occur, as the absorption intensity reached a maximum with 12 Cu(I). This is due presumably to the compactness of the Zn<sub>6–8</sub>-MTC structure and the ease for Cu(I) ions to form stable digonal and trigonal complexes.

In summary, the metal-binding properties of copper-specific *C. sapidus* MT (MTC) differ substantially from those of other crustacean MTs. In these MTs, a total of 18 Cys are involved in binding of six divalent metal ions [Zn(II) or Cd(II)] and up to ten Cu(I). However, in MTC well-defined M<sub>8</sub>-MTC complexes are formed with the divalent Zn(II) and Cd(II) and monovalent Cu(I) ions, involving all 21 Cys. In vivo studies showed that regardless of the metal supply (Cu or Zn and Cu) either homometallic Cu-MTC or heterometallic Zn,Cu-MTC were recovered in independent preparations, signifying that MTC may play a role in the metabolism of both metal ions. In this regard, the reversible uptake and release of two low-affinity Zn(II) ions from the two metal–thiolate clusters in Zn<sub>8</sub>-MTC would be consistent with such a function.

## Materials and methods

### Cloning of *C. sapidus* MTC cDNA

Crustacean MTC coding sequence (MTC cDNA), kindly provided by M. Brouwer of the University of Southern Mississippi, was cloned into pGEX-4T-1 expression vector. The coding sequence was amplified by PCR, using as a template the MTC cDNA inserted in a pGEM plasmid. The following oligonucleotides were used as PCR primers:

5'-GAAGATCTATGCCTTGTGGAT-3' (upstream primer)  
5'-CGGAATTCTTACTTCATTGGG-3' (downstream primer)

Through this reaction a *Bgl*III site was introduced immediately before the ATG initiation codon and an *Eco*RI site was introduced after the stop codon. The 30 cycles of PCR amplification were performed with Pwo polymerase (Roche Applied Science) under the following conditions: 94 °C for 30 s, 54 °C for 60 s, and 72 °C for 30 s. The PCR products were digested with *Bgl*III–*Eco*RI and subsequently cloned into the *Bam*HI–*Eco*RI sites of the pGEX-4T-1 expression vector (GE Healthcare). This strategy allowed us to keep the *Bam*HI restriction site intact in the MTC coding region. The DNA construct was confirmed by automatic DNA sequencing. The pGEX-4T-MTC plasmids were transformed into the *E. coli* protease-deficient strain BL21 for recombinant expression. As the presence of the rare Pro codon (CCC) could affect the amount and quality of protein produced in *E. coli*, the expression in BL21 Codon Plus RP *E. coli* strain (Stratagene), which contains extra copies of *proL* transfer RNA, was also assayed. The sodium dodecyl sulfate polyacrylamide gel electrophoresis analysis of protein extracts obtained from BL21 and BL21 Codon Plus RP cells, transformed by pGEX-4T-MTC, did not show any difference in recombinant protein levels; therefore, all the syntheses were performed in the protease-deficient BL21 *E. coli* strain.

### Expression and purification of the recombinant MTC protein as different metal complexes

Medium-scale cultures for analytical purposes (2 l) were grown in Erlenmeyer flasks, whereas large-scale cultures (50 l) for NMR studies were performed in a Biostat UD50 pilot-scale bioreactor. In both cases, the transformed *E. coli* BL21 cells were grown in Luria–Bertani medium supplemented with 100 µg ml<sup>-1</sup> ampicillin and one of the following metal salt supplements: 300 µM ZnCl<sub>2</sub> for zinc-enriched medium, 500 µM CuSO<sub>4</sub> for copper-enriched medium, and 300 µM ZnCl<sub>2</sub> plus 500 µM CuSO<sub>4</sub> for zinc- and copper-enriched medium. The cultures were induced with isopropyl 1-thio-β-D-galactopyranoside at a final

concentration of 100 µM. Purification of metal–MTC complexes was performed as described for mouse MT-1 [20]. After the gel filtration chromatography, samples were pooled and stored at –80 °C under an argon atmosphere until further analysis.

### Preparation and characterization of apoMTC

Vašák's method [44] provides a useful strategy to obtain fully loaded MTs via the previous purification of the corresponding apo form. Minor modifications to this method enabled us to recover apoMTC with a high degree of purity. Solutions containing 1–10 mg of recombinant Zn–MTC, in 20 mM tris(hydroxymethyl)aminomethane (Tris)–HCl (pH 7.5–8), were incubated for 45 min with 20 mol equiv of dithiothreitol per Cys residue and 4 M guanidine hydrochloride, under argon bubbling. Acidification of the solution to pH 1–1.5 was achieved by the addition of 6 M HCl. Centriprep YM-3 concentrators (Amicon) were used to concentrate the sample to 1–2 ml. Gel filtration through a Sephadex G-10 column (1.5 cm × 42 cm) equilibrated with 10 mM HCl and elution with the same solution (1 ml min<sup>-1</sup>) allowed removal of the Zn(II) ions released from Zn–MTC at low pH. The eluate was collected in 1-ml fractions and monitored for absorbance at 220 nm. The fractions corresponding to apoMTC were pooled. The protein concentration and the total metal content were determined by ICP-AES analysis. The apoMTC sample was kept at –80 °C until further use. ICP-AES and ESI-MS data indicated the absence of metals, and DTP reaction showed an oxidation degree lower than 5%. The CD (no bands at a wavelength higher than 220 nm) and UV (no bands at a wavelength higher than 240 nm) features were fully consistent with those of metal-free MTC.

The average acidity constant of the Cys residues in apoMTC and the molar extinction coefficient for a deprotonated Cys residue were calculated from the spectrophotometric titration with NaOH (Fig. S5) using a reported procedure [42]. Both values, pK<sub>a</sub> = 9.0 and ε<sub>237</sub> = 5 × 10<sup>3</sup> M<sup>-1</sup> cm<sup>-1</sup> per Cys, compare well with those reported for mammalian MTs [40].

### Reconstitution of apoMTC with Zn(II) or Cd(II)

Fully loaded Zn(II) or Cd(II) MTC was prepared by reconstitution following a slightly modified Vašák's method [44]. The solutions used were rendered oxygen-free by three freeze–pump–thaw cycles on a vacuum line and all sample preparation steps were performed in an argon-purged glove box. Both fully loaded Zn–MTC and Cd–MTC forms were obtained by the mixing of 8.5 mol equiv of ZnCl<sub>2</sub> or CdCl<sub>2</sub>, respectively, with apoMTC in 10 mM HCl. The solution mixture was then adjusted to pH

7 with 1 M Tris base and incubated overnight. Finally, a gel filtration chromatography was performed in an ÄKTA purifier (GE Healthcare) to remove the excess of metal ions. The Superdex-75 HR column was equilibrated with 10 mM Tris–HCl, pH 7.2 and run at 0.5 ml min<sup>−1</sup>.

#### Analytical and spectroscopic techniques

The sulfur, zinc, cadmium and copper content of apoMTC and holoMTC samples was analyzed by means of ICP-AES using a Polyscan 61E (Thermo Jarrell Ash) spectrometer, measuring sulfur at 182.040 nm, zinc at 213.856 nm, cadmium at 228.802 nm, and copper at 324.803 nm. The sample preparation was performed as already described [45]. To evaluate possible traces of labile sulfide ions in recombinant metal–MTC complexes, the corresponding samples were incubated in 1 M HCl at 65 °C for 5 min prior to measurements by ICP-AES [21]. For all samples, the protein concentration was calculated from the sulfur content determined by ICP-AES assuming that all sulfur atoms were contributed by the MTC peptide, i.e., 23 sulfur atoms per mole of MTC (two Met and 21 Cys residues).

The percentage of thiol groups in reduced form over the total sulfur content in the samples of apoMTC and reconstituted MTC was determined through the reaction of MTC with DTP in 0.2 M sodium acetate/1 mM EDTA (pH 4), which was followed spectroscopically using  $\epsilon_{343} = 7,600 \text{ M}^{-1} \text{ cm}^{-1}$  [38].

A JASCO spectropolarimeter (model J-715) interfaced to a computer (J700 software) was used for CD measurements. Electronic absorption measurements were performed with an HP-8453 diode-array UV–vis spectrophotometer. All spectra were recorded from samples in 1-cm capped quartz cuvettes, corrected for the dilution effects and processed using the GRAMS 32 program.

The molecular mass of holoMTC samples was determined by ESI-MS using an Ultima Micromass quadrupole time-of-flight instrument, controlled by MassLynx software and calibrated with NaI (0.2 g of NaI dissolved in 100 ml of a 1:1 H<sub>2</sub>O/2-propanol mixture). Samples of 20- $\mu\text{l}$  volume were injected at 40  $\mu\text{l min}^{-1}$  under the following conditions: source temperature, 100–150 °C; desolvation temperature, 150–250 °C; capillary counter electrode voltage, 3.0 kV; cone potential, 80 V. Spectra were collected throughout an  $m/z$  range from 950 to 2,000 at a rate of 2 s per scan with an interscan delay of 0.1 s. The liquid carrier was a 10:90 mixture of acetonitrile and 5 mM ammonium acetate, pH 7.

The same ESI-MS equipment was used to assess the correctness of recombinant Zn<sub>6–8</sub>–MTC. This was ascertained by determining the molecular mass of the corresponding apoMTC form, which was obtained by using a liquid carrier consisting of a 50:50 mixture of acetonitrile and ammonium formate/ammonia at pH 2.5. Also, the

source temperature was decreased to 100 °C and the desolvation temperature to 150 °C. The other experimental conditions were the same as described above. In all cases, molecular masses were theoretically calculated as previously described [46]. All samples were injected at least twice to ensure reproducibility.

Calculation of the average acidity constant of apoMTC and determination of the molar extinction coefficient for a deprotonated Cys residue

The spectrophotometric titration of apoMT with base is a common procedure to determine the acidity constants of the Cys thiol groups, and is based on the characteristic strong absorption band, between 230 and 240 nm, assigned to free thiolate ligands [40]. To ensure anaerobic conditions, sample preparation steps were performed in an argon-purged glove box. Thus, each point of the titration of apoMTC with 1 M NaOH was obtained from individual 12  $\mu\text{M}$  apoMTC in 10 mM HCl samples that were kept in sealed 1-cm quartz cuvettes [42]. Twenty-six spectra between 200 and 400 nm were taken within the pH range 2–11 and the pH was immediately determined using a microelectrode. The graphical representation of the absorbance at 237 nm as a function of the corresponding pH value shows a one-step titration curve and, thus, the pH of the inflection point can be assigned to an average  $\text{pK}_a$  value of the Cys residues [40]. The first derivative of the titration curve afforded a  $\text{pK}_a$  value of 8.9 (Fig. S5). The experimental data thus obtained were also analyzed by importing both the absorbance and the pH values into the pHab2000 computer program [47], which calculates acidity constants by means of a linear least-squares curve-fitting analysis. The best fit was obtained for an average apparent  $\text{pK}_a$  value of  $9.05 \pm 0.01$  for all Cys residues, which is consistent with literature data for other MTs [40, 42].

From the same data, the molar extinction coefficient per Cys thiolate group can be estimated by dividing the maximum molar extinction coefficient at 237 nm by the total number of Cys residues, i.e.,  $[\epsilon_{\text{thiolate (pH 11.0)}} - \epsilon_{\text{thiolate (pH 2.0)}}] / 21 = (1.1 \times 10^5) / 21$  was approximately  $5 \times 10^3 \text{ M}^{-1} \text{ cm}^{-1}$ . This value was used in the determination of the number of free Cys residues in holoMTC species as indicated later.

#### Chelex 100 treatment

Solutions of the reconstituted Zn<sub>6–8</sub>–MTC and Cd<sub>8</sub>–MTC forms were incubated overnight with Chelex 100 resin as already described [20]. During this time, the sample was constantly shaken and kept in an argon-purged glove box. Aliquots of the supernatant solution were analyzed by means of UV absorption, CD, and ESI-MS measurements.



### Determination of unbound Cys residues in holoMTC species

Zn<sub>6</sub>–MTC and Cd<sub>7</sub>–MTC obtained from the reconstituted Zn<sub>6–8</sub>–MTC and Cd<sub>8</sub>–MTC forms, respectively, after Chelex 100 treatment were titrated with NaOH up to pH higher than 11 and the absorption spectra at the different pH values were recorded from 400 to 200 nm [42]. The average free Cys content was calculated from the increase in the molar extinction coefficient at 237 nm of Zn<sub>6</sub>–MTC or Cd<sub>7</sub>–MTC, from neutral pH up to 11. This increment,  $\Delta\epsilon_{237} = 10^4 \text{ M}^{-1} \text{ cm}^{-1}$  for Zn<sub>6</sub>–MTC and  $3 \times 10^3 \text{ M}^{-1} \text{ cm}^{-1}$  for Cd<sub>7</sub>–MTC, divided by the already determined average molar extinction coefficient of the Cys thiolate in MTC,  $5 \times 10^3 \text{ M}^{-1} \text{ cm}^{-1}$  per Cys, was indicative of two free Cys residues in Zn<sub>6</sub>–MTC and at most one in Cd<sub>7</sub>–MTC.

### Determination of the apparent binding constant of Cd(II) bound to MTC

The apparent binding constant of Cd<sub>8</sub>–MTC at pH 7.0 was determined as previously described [38] by using an adapted expression of Wang et al. [42]. Briefly, the release of Cd(II) from Cd<sub>8</sub>–MTC is achieved by lowering the pH by the addition of increasing amounts of oxygen-free 1.0 M HCl. Prior to measurements, a stock solution of Cd<sub>8</sub>–MTC was diluted to a final concentration of 5  $\mu\text{M}$  in 10 mM Tris–HCl, 20 mM NaCl, pH 8.8, and rendered oxygen-free by three freeze–pump–thaw cycles on a vacuum line. The pH titration was performed on independent samples prepared in an argon-purged glove box. Metal release was followed by recording absorption spectra between 400 and 200 nm of a sample in a sealed 1-cm cuvette. The pH was determined using a microelectrode immediately after the spectra had been recorded. The degree of Cd(II) release is illustrated by plotting the pH values against the percentage of metal dissociation calculated by  $D = (\epsilon_{250,i} - \epsilon_{250,\text{pH } 2.2})/(\epsilon_{250,\text{pH } 8.8} - \epsilon_{250,\text{pH } 2.2})$ , where  $\epsilon_{250,i}$  is the molar extinction coefficient at 250 nm of the Cd(II)–thiolate complex at each pH value (*i*) and  $\epsilon_{250,\text{pH } 8.8}$  and  $\epsilon_{250,\text{pH } 2.2}$  correspond to Cd<sub>8</sub>–MTC (pH 8.8) and apoMTC (pH 2.2), respectively (Fig. S2). The pH titration profile of Cd<sub>8</sub>–MTC, as described for Cd<sub>7</sub>–MT-3 [41], did not display a pronounced two-step titration profile. Therefore, only the overall apparent binding constant was calculated using the following equation:  $K_{\text{app,pH } 7} = [\text{H}^+]^n/[\text{Cd}^{2+}] \times 10^{-7n}$ , where  $[\text{H}^+] = 10^{-3.3}$  and  $[\text{Cd}^{2+}] = 1.92 \times 10^{-5} \text{ M}$  denote the proton and Cd(II) concentrations at the titration midpoint value, respectively (Fig. S2). On the basis of the CysS-to-Cd(II) stoichiometry (21:8) the average number of thiolate ligands bound to Cd(II), *n*, was considered to be 2.6. From this equation, the  $K_{\text{app,pH } 7}$  value of  $2.2 \times 10^{14} \text{ M}^{-1}$  was obtained.

### Metal ion binding reactions

The sequential addition of Cu(I) to a solution of either Zn<sub>6–8</sub>–MTC at pH 7 or Zn<sub>6–8</sub>–MTC at pH 3 was monitored by UV and CD measurements. All manipulations were carried out in an argon atmosphere at room temperature and the pH was kept constant throughout the titration. The procedures followed in the preparation of concentrated  $[\text{Cu}(\text{MeCN})_4]\text{ClO}_4$  stock solution as well as for the UV and CD monitoring of the previously described titrations have already been described [20, 48]. In the various titrations, the initial protein concentration ranged between 10 and 20  $\mu\text{M}$ .

In the titration of apoMTC with Cu(I) a different procedure was followed to ensure strict anaerobic conditions. In this case, each point of the titration was obtained using independent samples. ApoMTC (9  $\mu\text{M}$ ) in 0.1 M HCl aliquots was titrated with increasing Cu(I) mole equivalents (0–18) in an argon-purged glove box followed by adjustment of the pH of the sample to 7.2 with 1 M Tris base. Subsequently, the ESI-MS spectrum of each aliquot was recorded.

Similarly to the titration with Cu(I), cadmium-binding studies were carried out using independent samples of apoMTC (9  $\mu\text{M}$ ) in 0.1 M HCl to which increasing CdCl<sub>2</sub> mole equivalents (0–10) were added in an argon-purged glove box. After each addition, the pH of the sample was adjusted to 7.2 with 1 M Tris. The CD and UV spectra were recorded in a sealed cuvette. Immediately afterward, the ESI-MS spectrum of the same sample was also recorded.

### NMR studies

Reconstitution of apoMTC with  $^{113}\text{CdCl}_2$ , obtained by treatment of  $^{113}\text{CdO}$  (TRACER Tecnologías Analíticas) with a stoichiometric amount of HCl, yielded  $^{113}\text{Cd}_8$ –MTC. On the basis of ESI-MS data, further treatment with Chelex 100 resin afforded  $^{113}\text{Cd}_7$ –MTC. Among the different attempts to obtain concentrated solutions, lyophilisation proved to be the most successful. The NMR measurements were performed at pH 6.5, using a 1 mM solution of the protein in 90% H<sub>2</sub>O/10% D<sub>2</sub>O with 10 mM perdeuterated Tris–HCl and 0.02% (w/v) sodium azide. To avoid protein oxidation, the reducing agent  $\beta$ -MeSH was also present at either low (0.5–1 mM) or high (10–30 mM) concentration.

$^1\text{H}$  homonuclear NMR experiments were acquired using Bruker Avance 600 and Bruker Avance 800 spectrometers operating at 11.74 and 18.78 T, respectively. The former was equipped with a triple-resonance TXI probe, whereas the latter had a triple-resonance TCI cryoprobe. The  $^1\text{H}$  homonuclear experiments were of the standard form and

were performed as previously described [49]. Three different mixing times (80, 200, and 400 ms) were used at different temperatures (5, 15, and 27 °C) in the nuclear Overhauser enhancement spectroscopy experiments. The MLEV-17 spin-lock applied for 70 or 160 ms was employed in the total correlation spectroscopy experiments.

Both the  $^{113}\text{Cd}$  direct detection and the heteronuclear  $^1\text{H}$ – $^{113}\text{Cd}$  HMQC experiments were acquired using Bruker Avance 400 (operating at 9.4 T) and Bruker Avance 600 (11.74 T) spectrometers. The  $^1\text{H}$  and  $^{113}\text{Cd}$  resonance frequencies were 400.13 (600.13) and 88.97 (133.19) MHz, respectively. BBO probes were used in  $^{113}\text{Cd}$  direct detections, whereas heteronuclear experiments were carried out with BBO probes (at 11.74 T) or BBI probes (9.4 T). Spectral windows of 400 ppm, 32,768 acquisition points,  $^1\text{H}$  decoupling with the WALTZ-16 pulse sequence, and recycle times of 1 s were typically used for  $^{113}\text{Cd}$  direct acquisition experiments. A total number of  $(1.2\text{--}1.5) \times 10^5$  scans, in blocks of 4,096 scans each, were acquired (i.e. approximately 1.5 days per 1D experiment). For heteronuclear experiments ( $^1\text{H}$ – $^{113}\text{Cd}$  HMQC), spectral windows of 10 and 150 ppm acquired with 2,048 and 200 complexes data points in the direct ( $^1\text{H}$ ) and evolution ( $^{113}\text{Cd}$ ) dimensions were used.  $^{113}\text{Cd}$  decoupling was achieved with the gap sequence. Solvent signal was eliminated by the WATERGATE sequence. Five hundred and twelve scans per increment were taken. The total duration of each experiment was approximately 1 day.  $^{113}\text{Cd}$  chemical shifts were referenced with respect to the signal of a 0.1 M sample of  $\text{Cd}(\text{ClO}_4)_2$ . The free-induction decays obtained were multiplied by a squared sine function ( $\pi/3$ -shifted in the direct dimension and without shifting in the  $^{113}\text{Cd}$  evolution). The final 2D spectra consisted of  $2,048 \times 256$  data points. All spectra were processed with the standard Bruker software (Topspin program) and analyzed with the program Sparky [50].

**Acknowledgments** The authors gratefully acknowledge financial support from DURSI, Generalitat de Catalunya (SGR2009-68), Fundación Séneca de la Región de Murcia (05716/PI/07), and the Spanish Ministerio de Ciencia e Innovación (CTQ2008-02767/BQU). L.A.A is indebted to the Program Juan de la Cierva (Ministerio de Ciencia e Innovación, Spain). We are grateful to Marius Brouwer (Institute of Marine Sciences, University of Southern Mississippi, USA) who kindly provided the *C. sapidus* MTC cDNA clone. The authors thank the NMR Facility of the Serveis Científicotècnics of the Universitat de Barcelona for providing access to the 800-MHz NMR spectrometer.

## References

- González-Duarte P (2003) In: McCleverty J, Meyer TJ (eds) Comprehensive coordination chemistry II, vol 8. Elsevier-Peramon, Amsterdam, pp 213–228
- Vášák M, Romero-Isart N (2006) In: King RB (ed) Encyclopedia of inorganic chemistry. Wiley, New York, pp 3208–3221
- Blindauer CA, Harrison MD, Parkinson JA, Robinson AK, Cavet JS, Robinson NJ, Sadler PJ (2001) Proc Natl Acad Sci USA 98:9593–9598
- Peroza EA, Schmucki R, Guntert P, Freisinger E, Zerbe O (2009) J Mol Biol 387:207–218
- Hong SH, Maret W (2003) Proc Natl Acad Sci USA 100:2255–2260
- Gruber C, Sturzenbaum S, Gehrig P, Sack R, Hunziker P, Berger B, Dallinger R (2000) Eur J Biochem 267:573–582
- Moltó E, Bonzón-Kulichenko E, Gallardo N, Andrés A (2007) Arch Biochem Biophys 467:31–40
- Díaz S, Amaro F, Rico D, Campos V, Benítez L, Martín-González A, Hamilton EP, Orias E, Gutiérrez JC (2007) PLoS One. doi:10.1371/journal.pone.0000291
- Park H, Ahn IY, Choi HJ, Pyo SH, Lee HE (2007) Protein Exp Purif 52:82–88
- Jenny MJ, Warr GW, Ringwood AH, Baltzegar DA, Chapman RW (2006) Gene 379:156–165
- Syring RA, Brouwer-Hoexum T, Brouwer M (2000) Comp Biochem Physiol C Toxicol Pharmacol 125:325–332
- García S, Prado M, Degano R, Domínguez A (2002) J Biol Chem 277:37359–37368
- Domènech J, Bofill R, Tinti A, Torreggiani A, Atrian S, Capdevila M (2008) Biochim Biophys Acta 1784:693–704
- Narula SS, Brouwer M, Hua Y, Armitage IM (1995) Biochemistry 34:620–631
- Muñoz A, Forsterling FH, Shaw CF III, Petering DH (2002) J Biol Inorg Chem 7:713–724
- Brouwer M, Brouwer-Hoexum T (1998) Arch Biochem Biophys 351:257–264
- Yudkovski Y, Shechter A, Chalifa-Caspi V, Auslander M, Ophir R, Dauphin-Villemant C, Waterman M, Sagi A, Tom M (2007) Insect Mol Biol 16:661–674
- Cols N, Romero-Isart N, Capdevila M, Oliva B, González-Duarte P, González-Duarte R, Atrian S (1997) J Inorg Biochem 68:157–166
- Valls M, Bofill R, González-Duarte R, González-Duarte P, Capdevila M, Atrian S (2001) J Biol Chem 276:32835–32843
- Capdevila M, Cols N, Romero-Isart N, González-Duarte R, Atrian S, González-Duarte P (1997) Cell Mol Life Sci 53:681–688
- Capdevila M, Domenech J, Pagani A, Tio L, Villarreal L, Atrian S (2005) Angew Chem Int Ed 44:4618–4622
- Birchmeier W, Christen P (1971) FEBS Lett 18:209–213
- Overnell J, Good M, Vášák M (1988) Eur J Biochem 172:171–177
- Brouwer M, Syring R, Brouwer-Hoexum T (2002) J Inorg Biochem 88:228–239
- Brouwer M, Schlenk D, Ringwood AH, Brouwer-Hoexum T (1992) Arch Biochem Biophys 294:461–468
- Pagani A, Villarreal L, Capdevila M, Atrian S (2007) Mol Microbiol 63:256–269
- Tio L, Villarreal L, Atrian S, Capdevila M (2004) J Biol Chem 279:24403–24413
- Brouwer M (1996) Adv Inorg Biochem 11:235–260
- Dance IG, Fisher K, Lee G (1992) In: Stillman MJ, Shaw III CF, Suzuki KT (eds) Metallothioneins. VCH, New York, pp 284–345
- Calderone V, Dolderer B, Hartmann HJ, Echner H, Luchinat C, Del Bianco C, Mangani S, Weser U (2005) Proc Natl Acad Sci USA 102:51–56
- Dallinger R, Chabicovalsky M, Hodl E, Prem C, Hunziker P, Manzl C (2005) Am J Physiol Regul Integr Comp Physiol 289:R1185–R1195

32. Jensen LT, Peltier JM, Winge D (1998) *J Biol Inorg Chem* 3:627–631
33. Zhang L, Pickering IJ, Winge DR, George GN (2008) *Chem Biodivers* 5:2042–2049
34. Roschitzki B, Vašák M (2002) *J Biol Inorg Chem* 7:611–616
35. Pountney DL, Schauwecker I, Zarn J, Vašák M (1994) *Biochemistry* 33:9699–9705
36. Graslund S, Nordlund P, Weigelt J, Hallberg BM, Bray J, Gileadi O, Knapp S, Oppermann U, Arrowsmith C, Hui R, Ming J, dhe-Paganon S, Park HW, Savchenko A, Yee A, Edwards A, Vincentelli R, Cambillau C, Kim R, Kim SH, Rao Z, Shi Y, Terwilliger TC, Kim CY, Hung LW, Waldo GS, Peleg Y, Albeck S, Unger T, Dym O, Prilusky J, Sussman JL, Stevens RC, Lesley SA, Wilson IA, Joachimiak A, Collart F, Dementieva I, Donnelly MI, Eschenfeldt WH, Kim Y, Stols L, Wu R, Zhou M, Burley SK, Emtage JS, Sauder JM, Thompson D, Bain K, Luz J, Gheyi T, Zhang F, Atwell S, Almo SC, Bonanno JB, Fiser A, Swaminathan S, Studier FW, Chance MR, Sali A, Acton TB, Xiao R, Zhao L, Ma LC, Hunt JF, Tong L, Cunningham K, Inouye M, Anderson S, Janjua H, Shastry R, Ho CK, Wang D, Wang H, Jiang M, Montelione GT, Stuart DI, Owens RJ, Daenke S, Schutz A, Heinemann U, Yokoyama S, Bussow K, Gunsalus KC (2008) *Nat Methods* 5:135–146
37. Hennehan CJ, Pountney DL, Zerbe O, Vašák M (1993) *Protein Sci* 2:1756–1764
38. Meloni G, Zovo K, Kazantseva J, Palumaa P, Vašák M (2006) *J Biol Chem* 281:14588–14595
39. Peroza EA, Kaabi AA, Meyer-Klaucke W, Wellenreuther G, Freisinger E (2009) *J Inorg Biochem* 103:342–353
40. Vašák M, Kagi JHR (1983) In: Sigel H (ed) *Spectroscopic properties of metallothioneins. Metal ions in biological systems*, vol 15. Dekker, New York, pp 213–273
41. Hasler DW, Jensen LT, Zerbe O, Winge DR, Vašák M (2000) *Biochemistry* 39:14567–14575
42. Wang Y, Mackay EA, Kurasaki M, Kagi JH (1994) *Eur J Biochem* 225:449–457
43. Willner H, Vašák M, Kagi JH (1987) *Biochemistry* 26:6287–6292
44. Vašák M (1991) In: Riordan JF, Vallee BL (eds) *Metal removal and substitution in vertebrate and invertebrate metallothioneins. Methods in enzymology*, vol 205, metallobiochemistry. Academic Press, San Diego, pp 452–458
45. Bongers J, Walton CD, Richardson DE, Bell JU (1988) *Anal Chem* 60:2683–2686
46. Fabris D, Zaia J, Hathout Y, Fenselau C (1996) *J Am Chem Soc* 118:12242–12243
47. Gans P, Sabatini A, Vacca A (1999) *Ann Chim* 89:45–49
48. Bofill R, Palacios O, Capdevila M, Cols N, González-Duarte R, Atrian S, González-Duarte P (1999) *J Inorg Biochem* 73:57–64
49. Donaire A, Zhou ZH, Adams MM, La Mar GN (1996) *J Biomol NMR* 7:35–47
50. Goddard TD, Kneller DG *SPARKY 3—NMR assignment program*. University of California, San Francisco